

# End-to-End differentiable construction of molecular mechanics force fields

Yuanqing Wang (ORCID: [0000-0003-4403-2015](https://orcid.org/0000-0003-4403-2015))<sup>1, 3, 4</sup>,

Josh Fass (ORCID: [0000-0003-3719-266X](https://orcid.org/0000-0003-3719-266X))<sup>1, 2†</sup>,

John D. Chodera (ORCID: [0000-0003-0542-119X](https://orcid.org/0000-0003-0542-119X))<sup>1</sup>

<sup>1</sup>Computational and Systems Biology Program, Sloan Kettering Institute, Memorial Sloan Kettering Cancer Center, New York, NY 10065; <sup>2</sup>Tri-Institutional PhD Program in Computational Biology and Medicine, Weill Cornell Medical College, Cornell University, New York, NY 10065; <sup>3</sup>Physiology, Biophysics, and System Biology Ph.D. Program, Weill Cornell Medical College, Cornell University, New York, NY 10065; <sup>4</sup>MFA. Program in Creative Writing, Division of Humanities and Arts, the City College of New York, the City University of New York, New York, NY 10031

**\*For correspondence:**

[yuanqing.wang@choderalab.org](mailto:yuanqing.wang@choderalab.org) (YW); [john.chodera@choderalab.org](mailto:john.chodera@choderalab.org) (JDC)

**Present address:** <sup>5</sup>Relay Therapeutics, Cambridge, MA 02139

---

**Abstract** Molecular mechanics (MM) potentials have long been a workhorse of computational chemistry. Leveraging accuracy and speed, these functional forms find use in a wide variety of applications in biomolecular modeling and drug discovery, from rapid virtual screening to detailed free energy calculations. Traditionally, MM potentials have relied on human-curated, inflexible, and poorly extensible discrete chemical perception rules (*atom types*) for applying parameters to small molecules or biopolymers, making it difficult to optimize both types and parameters to fit quantum chemical or physical property data. Here, we propose an alternative approach that uses *graph neural networks* to perceive chemical environments, producing continuous atom embeddings from which valence and nonbonded parameters can be predicted using invariance-preserving layers. Since all stages are built from smooth neural functions, the entire process—spanning chemical perception to parameter assignment—is modular and end-to-end differentiable with respect to model parameters, allowing new force fields to be easily constructed, extended, and applied to arbitrary molecules. We show that this approach is not only sufficiently expressive to reproduce legacy atom types, but that it can learn and extend existing molecular mechanics force fields and construct entirely new force fields applicable to both biopolymers and small molecules from quantum chemical calculations, and even learn to accurately predict free energies from experimental observables. This approach is implemented in the free and open source package **Espaloma**, available at <https://github.com/choderalab/espaloma>.

---

Molecular mechanics force fields—physical models that abstract molecular systems as atomic point masses that interact via nonbonded interactions and valence (bond, angle, torsion) terms—have powered *in silico* modeling to provide key insights and quantitative predictions in all aspects of chemistry, from drug discovery to materials science [1–9]. While recent work in quantum machine learning (QML) potentials has demonstrated how flexibility in functional forms and training strategies can lead to increased accuracy [10–15], these QML potentials are orders of magnitude slower than popular molecular mechanics potentials, since the learned neural function must be evaluated and differentiated during simulation. On the other

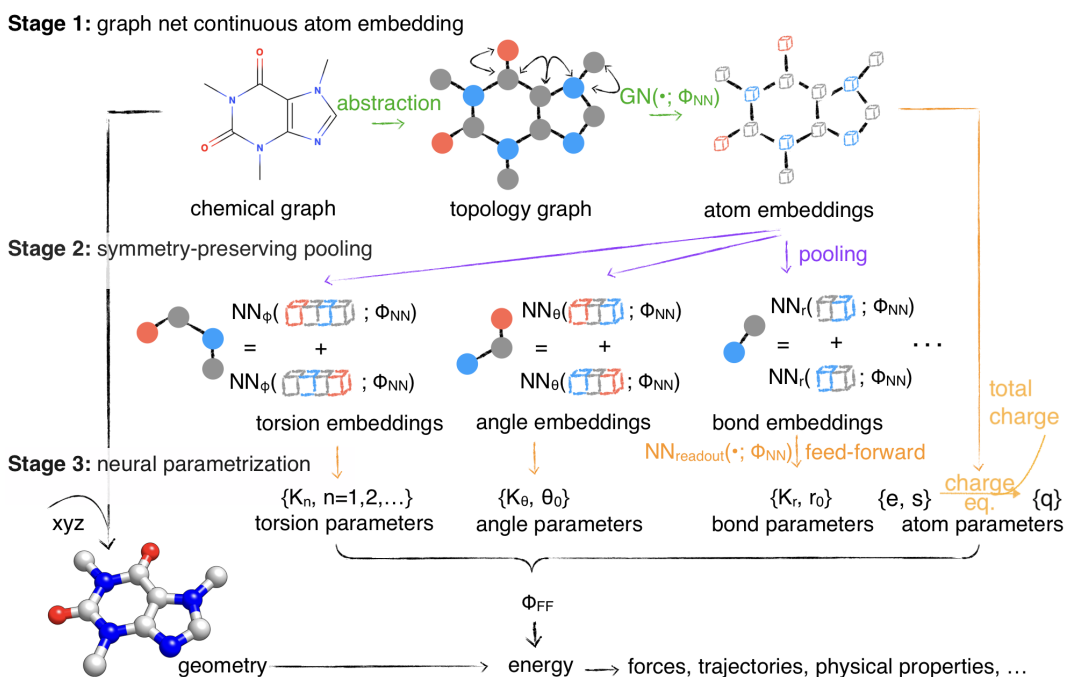


**Figure 1. End-to-end differentiable molecular mechanics parameter assignment.** Espaloma (*extendable surrogate potential optimized by message-passing*) is a modular approach for directly computing molecular mechanics force field parameters  $\Phi_{FF}$  from a chemical graph  $\mathcal{G}$  such as a small molecule or biopolymer via a process that is fully differentiable in the model parameters  $\Phi_{NN}$ . In **Stage 1**, a graph neural network is used to generate continuous latent atom embeddings describing local chemical environments from the chemical graph. In **Stage 2**, these atom embeddings are transformed into feature vectors that preserve appropriate symmetries for atom, bond, angle, and proper/improper torsion inference via Janossy pooling. In **Stage 3**, molecular mechanics parameters are directly predicted from these feature vectors using feed-forward neural nets. This parameter assignment process is performed once per molecular species, allowing the potential energy to be rapidly computed using standard molecular mechanics implementations thereafter. The collection of parameters  $\Phi_{NN}$  describing the Espaloma model can be considered as the equivalent of a traditional molecular mechanics force field, in that it encodes the equivalent of traditional typing rules and parameter assignment tables. This final stage is modular, and can be easily extended to incorporate additional molecular mechanics parameter classes, such as parameters for a charge-equilibration model (Section 6), point polarizabilities, or valence-coupling terms.

hand, the simpler physical energy functions of molecular mechanics (MM) models are compatible with highly optimized implementations that can exploit a variety of hardware [2, 16–20], but rely on complex and inextensible legacy *atom typing schemes* for parameter assignment [21]:

- First, a set of rules are used to classify atoms into discrete *atom types* that must encode all information about an atom’s chemical environment needed in subsequent parameter assignment steps.
- Next, a discrete set of bond, angle, and torsion types are determined by composing the atom types involved in the interaction.
- Finally, the parameters attached to atoms, bonds, angles, and torsions are assigned according to a look-up table of composed these parameter types.

As a result, atoms, bonds, angles, or torsions with distinct chemical environments that happen to fall into the same expert-derived discrete type class are forced to share a same set of MM parameters, potentially leading to poor accuracy. Furthermore, the explosion of discrete parameter classes describing equivalent chemical environments required by traditional MM atom typing schemes not only poses significant challenges to extending the space of atom types [21], optimizing these independently has the potential to compromise generalizability and lead to overfitting. Even with modern MM parameter optimization frameworks [22–24] and sufficient data, parameter optimization is only possible in the continuous parameter space defined by these fixed atom types, while the mixed discrete-continuous optimization problem—jointly optimizing types and parameters—is intractable.

Here, we demonstrate a continuous alternative to traditional discrete atom typing schemes that permits full *end-to-end differentiable optimization* of both typing and parameter assignment stages, allowing the entire force field to be built, extended, and applied using standard automatic differentiation machine learning frameworks such as PyTorch [25], TensorFlow [26], and JAX [27] (**Figure 1**). Graph neural networks have recently emerged as a powerful way to learn chemical properties of atoms, bonds, and molecules for biomolecular species (both small organic molecules and biopolymers), which can be considered isomorphic with their graph representations [28–37]. We hypothesize that graph neural networks operating on molecules have expressiveness that is at least equivalent to—and likely much greater than—expert-derived typing rules, with the advantage of being able to smoothly interpolate between representations of chemical environments (such as accounting for fractional bond orders [38]).

We first provide experimental evidence of this hypothesis by showing that, within acceptable errors:

- Graph neural networks can recover legacy atom types in a supervised classification task (Section 3).
- Graph neural networks, when combined with appropriate pooling functions and a subsequent prediction stage, can learn existing force fields when trained to fit the corresponding MM energies and forces, and generalize this force field to new molecules (Section 4).

Next, we demonstrate the utility of such a model (which we call the *extendable surrogate potential optimized by message-passing*, or **Espaloma**) to construct end-to-end optimizable force fields with continuous atom types. Espaloma assigns molecular mechanics parameters from a molecular graph in three differentiable stages (Figure 1):

- **Stage 1:** Continuous atom embeddings are constructed using graph neural networks to perceive chemical environments (Section 2.1).
- **Stage 2:** Continuous bond, angle, and torsion embeddings are constructed using pooling that preserves appropriate symmetries (Section 2.2).
- **Stage 3:** Molecular mechanics force field parameters are computed from atom, bond, angle, and torsion embeddings using feed-forward networks (Section 2.3).

Additional molecular mechanics parameter classes (such as point polarizabilities, valence coupling terms, or even parameters for charge-transfer models [39]) can easily be added in a modular manner. Like legacy molecular mechanics parameter assignment infrastructures, molecular mechanics parameters are assigned *once* for each system, and can be subsequently used to compute energies and forces or carry out molecular simulations with standard molecular mechanics packages.

Unlike traditional legacy force fields, however, Espaloma model parameters  $\Phi_{\text{NN}}$ —which define the entire *process* by which molecular mechanics force field parameters  $\Phi_{\text{FF}}$  are applied to any given molecule—can be easily re-fit to data from scratch in a variety of ways using standard, highly portable, high-performance machine learning frameworks that support automatic differentiation. Here, we show how Espaloma can be used to directly fit quantum chemical data to produce a complete force field (Section 5).

## 1 A graph theoretic view of Class I molecular mechanics force fields

Consider a molecular graph  $\mathcal{G}$  where atoms map to vertices  $\mathcal{V}$  and covalent bonds map to edges  $\mathcal{E}$ . In a class I molecular mechanics force field [40–46], the parameters  $\Phi_{\text{FF}}$  assigned to a molecule graph  $\mathcal{G}$  define how the total potential energy of a conformation  $\mathbf{x} \in \mathbb{R}^{|\mathcal{G}| \times 3}$  is computed from independent bond, angle, torsion, and nonbonded energy terms given the complete set of molecular mechanics parameters  $\Phi_{\text{FF}}$ .

$$\begin{aligned}
 U_{\text{MM}}(\mathbf{x}; \mathcal{G}, \Phi_{\text{FF}}) &= \sum_{(v_i, v_j) \in \mathcal{G}_{\text{bond}}} U_{\text{bond}}(r(\mathbf{x}; v_i, v_j); K_r(\Phi_{\text{FF}}; v_i, v_j), r_0(\Phi_{\text{FF}}; v_i, v_j)) \\
 &+ \sum_{(v_i, v_j, v_k) \in \mathcal{G}_{\text{angle}}} U_{\text{angle}}(\theta(\mathbf{x}; v_i, v_j, v_k); K_\theta(\Phi_{\text{FF}}; v_i, v_j, v_k), \theta_0(\Phi_{\text{FF}}; v_i, v_j, v_k)) \\
 &+ \sum_{(v_i, v_j, v_k, v_l) \in \mathcal{G}_{\text{torsion}}} U_{\text{torsion}}(\phi(\mathbf{x}; v_i, v_j, v_k, v_l); \{K_{\phi_n}(\Phi_{\text{FF}}; v_i, v_j, v_k, v_l)\}_{n=1}^{n_{\text{max}}}, \phi_0(\Phi_{\text{FF}}; v_i, v_j, v_k, v_l)) \\
 &+ \sum_{(v_i, v_j) \in \mathcal{G}_{\text{Coulomb}}} U_{\text{Coulomb}}(r(\mathbf{x}; v_i, v_j); q(\Phi_{\text{FF}}; v_i), q(\Phi_{\text{FF}}; v_j)) \\
 &+ \sum_{(v_i, v_j) \in \mathcal{G}_{\text{van der Waals}}} U_{\text{van der Waals}}(r(\mathbf{x}; v_i, v_j); \sigma(\Phi_{\text{FF}}; v_i, v_j), \epsilon(\Phi_{\text{FF}}; v_i, v_j))
 \end{aligned} \tag{1}$$

Here, the sets  $\mathcal{G}_{\text{bond}}$ ,  $\mathcal{G}_{\text{angle}}$ ,  $\mathcal{G}_{\text{torsion}}$  denote the duples, triples, and quadruples of bonded atoms (vertices) in  $\mathcal{G}$ , while  $\mathcal{G}_{\text{Coulomb}}$  and  $\mathcal{G}_{\text{van der Waals}}$  denotes the set of atom (vertex) pairs separated by at least *three* edges, since interactions separated by fewer edges are generally excluded.  $\epsilon_0$  denotes the vacuum electric permittivity. The potential terms depend on distances  $r(\mathbf{x}; v_i, v_j)$ , angles  $\theta(\mathbf{x}; v_i, v_j, v_k)$ , and torsions (dihedral angles)  $\phi(\mathbf{x}; v_i, v_j, v_k, v_l)$  measured for the corresponding atoms from the positions vector  $\mathbf{x}$ . The various parameter functions—bond force constant  $K_r$  and equilibrium distance  $r_0$ , angle force constant  $K_\theta$  and equilibrium angle  $\theta_0$ , periodic torsion term barrier height  $K_{\phi,n}$  and phase  $\phi_0$  for periodicity  $n$ , partial charge  $q$ , Lennard-Jones radius  $\sigma$  and well depth  $\epsilon$ —extract the parameters corresponding to specific sets of atoms (vertices) from the vector of molecular mechanics parameters  $\Phi_{\text{FF}}$  to compute that contribution to the total potential energy.

The individual potential energy terms are computed by functions that generally take simple harmonic or periodic forms with respect to bond lengths and angles in terms of the parameters for those specific interactions:

$$U_{\text{bond}}(r; K_r, r_0) = \frac{K_r}{2}(r - r_0)^2 \quad (2)$$

$$U_{\text{angle}}(\theta; K_\theta, \theta_0) = \frac{K_\theta}{2}(\theta - \theta_0)^2 \quad (3)$$

$$U_{\text{torsion}}(\phi; \{K_{\phi,n}\}, \phi_0) = \sum_{n=1}^{n_{\text{max}}} K_{\phi,n} [1 + \cos(n\phi)] \quad (4)$$

$$U_{\text{Coulomb}}(r; q_i, q_j) = \frac{1}{4\pi\epsilon_0} \frac{q_i q_j}{r} \quad (5)$$

$$U_{\text{van der Waals}}(r; \sigma, \epsilon) = 4\epsilon \left[ \left(\frac{\sigma}{r}\right)^{12} - \left(\frac{\sigma}{r}\right)^6 \right] \quad (6)$$

where  $K_r$  and  $K_\theta$  denote force constants for bonds and angles,  $r_0$  and  $\theta_0$  denote equilibrium bond lengths and angles,  $K_{\phi,n}$  denotes a torsion energy factor (which can be positive or negative) for periodicity  $n$ ,  $\epsilon_0$  is the permittivity of free space, and  $q_i$  denote partial charges. For force fields like AMBER [47] and CHARMM [48], the effective Lennard-Jones well depth  $\epsilon_{v_i, v_j}$  and radius  $\sigma_{v_i, v_j}$  parameters for an interacting pair of atoms are computed from atomic parameters for atoms  $v_i$  and  $v_j$  using Lorentz-Berthelot combining rules [49],

$$\sigma(\Phi_{\text{FF}}; v_i, v_j) = \frac{1}{2}(\sigma_{v_i} + \sigma_{v_j}) \quad (7)$$

$$\epsilon(\Phi_{\text{FF}}; v_i, v_j) = \sqrt{\epsilon_{v_i} \epsilon_{v_j}} \quad (8)$$

though alternative combining rules [50] or even pair-specific parameters [51] are also possible.

Typically, atom type based force field parameterization engines [21] such as those used in AMBER [47] or CHARMM [48] assign parameters based on templates (for biopolymer residues or solvents) or through chemical perception algorithms (as in the case of GAFF [52, 53] or CGenFF [54, 55]). More recently, an approach to assigning atom, bond, angle, and torsion parameters directly based on the common SMARTS/SMIRKS chemical perception language was introduced, which bypasses the need to define parameter classes in terms of atom types, but still retains discrete interaction types [21]. Automatically fitting these type definitions still represents an intractable mixed discrete-continuous optimization problem. In the next section, we will show how a continuous, differentiable model can assign parameters directly, without the use of discrete atom or interaction types.

## 2 Espaloma: End-to-end differentiable MM parameter assignment

In this section, we describe how our proposed framework, **Espaloma** (Figure 1), operates analogously to legacy force field typing schemes to generate MM parameters  $\Phi_{\text{FF}}$  from a molecular graph  $\mathcal{G}$  and neural model parameters  $\Phi_{\text{NN}}$ ,

$$\Phi_{\text{FF}} \leftarrow \text{Espaloma}(\mathcal{G}, \Phi_{\text{NN}}), \quad (9)$$

which can subsequently be used to compute the MM energy (as in Equation 1) for any conformation.

---

```
import torch, dgl, espaloma as esp

# retrieve OpenFF Gen2 Optimization Dataset
dataset = esp.data.dataset.GraphDataset.load("gen2").view(batch_size=128)

# define Espaloma stage I: graph -> atom latent representation
representation = esp.nn.Sequential(
    layer=esp.nn.layers.dgl_legacy.gn("SAGEConv"), # use SAGEConv implementation in DGL
    config=[128, "relu", 128, "relu", 128, "relu"], # 3 layers, 128 units, ReLU activation
)

# define Espaloma stage II and III:
# atom latent representation -> bond, angle, and torsion representation and parameters
readout = esp.nn.readout.janossy.JanossyPooling(
    in_features=128, config=[128, "relu", 128, "relu", 128, "relu"],
    out_features={
        # define modular MM parameters Espaloma will assign
        1: {"e": 1, "s": 1}, # atom hardness and electronegativity
        2: {"log_coefficients": 2}, # bond linear combination, enforce positive
        3: {"log_coefficients": 3}, # angle linear combination, enforce positive
        4: {"k": 6}, # torsion barrier heights (can be positive or negative)
    },
)

# compose all three Espaloma stages into an end-to-end model
espaloma_model = torch.nn.Sequential(
    representation, readout, esp.nn.readout.janossy.ExpCoefficients(),
    esp.mm.geometry.GeometryInGraph(), esp.mm.energy.EnergyInGraph(),
    esp.nn.readout.charge_equilibrium.ChargeEquilibrium(),
)

# define training metric
metrics = [
    esp.metrics.GraphMetric(
        base_metric=torch.nn.MSELoss(), # use mean-squared error loss
        between=['u', "u_ref"], # between predicted and QM energies
        level="g", # compare on graph level
    )
    esp.metrics.GraphMetric(
        base_metric=torch.nn.MSELoss(), # use mean-squared error loss
        between=['q', "q_hat"], # between predicted and reference charges
        level="n1", # compare on node level
    )
]

# fit Espaloma model to training data
results = esp.Train(
    ds_tr=dataset, net=espaloma_model, metrics=metrics,
    device=torch.device('cuda:0'), n_epochs=5000,
    optimizer=lambda net: torch.optim.Adam(net.parameters(), 1e-3), # use Adam optimizer
).run()

torch.save(espaloma_model, "espaloma_model.pt") # save model
```

---

**Listing 1.** Defining and training a modular Espaloma model.

## 2.1 Stage 1: Graph neural networks generate a continuous atom embedding, replacing legacy discrete atom typing

We propose to use graph neural networks [28–37] as a replacement for the rule-based chemical environment perception [21]. These neural architectures learn a useful representation of the atomic chemical environment from simple input features by updating and pooling embedding vectors via message passing rounds to neighboring atoms [37]. As such, symmetries in chemical graphs (chemical equivalencies) are inherently preserved, while a rich, continuous, and differentiable learnable representation of the atom environment is derived.

### 2.1.1 A brief introduction to graph neural networks

In the context of molecular machine learning, molecules are modelled as undirected graphs of bonded atoms, where each atom and bond can carry attributes reflecting their chemical nature from which complex chemical features can be learned. If we write this as a tuple of three sets,

$$\mathcal{G} = \{\mathcal{V}, \mathcal{E}, \mathcal{U}\} \quad (10)$$

Here,  $\mathcal{V}$  is the set of the vertices (or nodes) (atoms),  $\mathcal{E}$  the set of edges (bonds), and  $\mathcal{U} = \{\mathbf{u}\}$  the universal (global) attribute.

In a graph neural network (GN) a set of functions (with learnable parameters  $\Phi_{\text{NN}}$ ) govern the three stages used in both training and inference of a graph neural network: *initialization*, *propagation*, and *readout*. Following one of the most general description of the message-passing procedure in the propagation stage in [31], we briefly review the message-passing steps in graph neural networks, where node attributes  $\mathbf{v}$ , edge attributes  $\mathbf{e}$ , and global attributes  $\mathbf{u}$  are updated according to:

$$\mathbf{e}_k^{(t+1)} = \phi^e(\mathbf{e}_k^{(t)}, \sum_{i \in \mathcal{N}_k^e} \mathbf{v}_i, \mathbf{u}^{(t)}), \quad \text{edge update} \quad (11)$$

$$\bar{\mathbf{e}}_i^{(t+1)} = \rho^{e \rightarrow v}(E_i^{(t+1)}), \quad \text{edge-to-node aggregate} \quad (12)$$

$$\mathbf{v}_i^{(t+1)} = \phi^v(\bar{\mathbf{e}}_i^{(t+1)}, \mathbf{v}_i^{(t)}, \mathbf{u}^{(t)}), \quad \text{node update} \quad (13)$$

$$\bar{\mathbf{e}}^{(t+1)} = \rho^{e \rightarrow u}(E^{(t+1)}), \quad \text{edge-to-global aggregate} \quad (14)$$

$$\bar{\mathbf{u}}^{(t+1)} = \rho^{v \rightarrow u}(V^{(t)}), \quad \text{node-to-global aggregate} \quad (15)$$

$$\mathbf{u}^{(t+1)} = \phi^u(\bar{\mathbf{e}}^{(t+1)}, \bar{\mathbf{v}}^{(t+1)}, \mathbf{u}^{(t)}), \quad \text{global update} \quad (16)$$

where  $E_i = \{\mathbf{e}_k, k \in \mathcal{N}_i^v\}$  is the set of attributes of edges connected to a specific node,  $E_k = \{\mathbf{e}_k, k \in 1, 2, \dots, N^e\}$  is the set of attributes of all edges,  $V$  is the set of attributes of all nodes, and  $\mathcal{N}^v$  and  $\mathcal{N}^e$  denote the set of indices of entities connected to a certain node or a certain edge, respectively.  $\phi^e$ ,  $\phi^v$ , and  $\phi^u$  are update functions that take the *environment* of the an entity as input and update the attribute of the entity, which could be stateful or not;  $\rho^{e \rightarrow v}$ ,  $\rho^{e \rightarrow u}$ , and  $\rho^{v \rightarrow u}$  are aggregation functions that aggregate the attributes of multiple entities into an *aggregated* attribute which shares the same dimension with each entity. Note that it is common that the edges do not hold attribute but only pass messages onto neighboring nodes. For all models we survey here, edge-to-global update does not apply and global attribute does not present until the readout stage, when a sum function is applied to form the global representation ( $\mathbf{u} = \sum_i \mathbf{v}_i$ ). We review the specifics of the graph neural network architectures that we considered here in the Appendix (Table 4).

### 2.1.2 Graph neural networks can replace discrete atom typing schemes by learning continuous atom environment embeddings

The traditional assignment of discrete atom types (for example, assignment of GAFF parameters via Antechamber [52, 53]) considers the element identity, hybridization, and aromaticity of the atom of interest as well as its neighbors. It closely resembles a two- or three-step Weisfeiler-Leman test [56], which has been shown to be approximated by some graph neural network architectures [28]. We therefore hypothesize that these graph neural network architectures can be at least as expressive as legacy atom typing rules. Although such a statement is difficult to prove theoretically due to the irregular and diverse grammar used in legacy force fields, we offer experimental evidence of this conjecture in Section 3.

To compute continuous atom embeddings, we start with a molecular graph  $\mathcal{G}$  whose atoms (nodes) are labeled with simple chemical properties (here, we consider element, hybridization, aromaticity, and formal charge, and membership in various ring sizes) easily computed in any cheminformatics toolkit. Sequential application of the graph neural network message-passing update rules (Section 2.1.1) then computes an updated set of atom (node) features in each graph neural network layer, and the final atom embeddings  $h_v \in \mathbb{R}^{|\mathcal{G}| \times D}$  are extracted from the final layer.

The benefits of neural embedding compared to legacy discrete typing are many-fold:

- Legacy typing schemes are generally described in text form in published work (for example [52, 53]), creating the potential for discrepancies between implementations when different cheminformatics toolkits are used. By contrast, with the *knowledge* to distinguish chemical environments stored in latent vectors and not dependent on any manual coding, our approach is deterministic once trained, and is portable across platforms thanks to modern machine learning frameworks.
- Both the chemical perception process and the application of force field parameters  $\Phi_{\text{FF}}$  can be optimized simultaneously via gradient-based optimization of  $\Phi_{\text{NN}}$  using standard machine learning frameworks that support automatic differentiation.
- While extending a legacy force field by adding new atom types can lead to an explosion in the number of parameter types, continuous neural embeddings do not suffer from this limitation; expansion of the typing process occurs automatically as more diverse training examples are introduced.

## 2.2 Stage 2: Symmetry-preserving pooling generates continuous bond, angle, and torsion embeddings, replacing discrete types

Many terms in a molecular mechanics potential are symmetric with respect to certain permutations of the atoms involved in the interaction. For example, harmonic bond terms are symmetric with respect to the exchange of atoms involved in the bond. More elaborate symmetries are frequently present, such as in the three-fold terms representing improper torsions for the Open Force Field "Parsley" generation of force fields ( $k - i - j - l$ ,  $k - j - l - i$ , and  $k - l - i - j$ , where  $k$  is the central atom) [57]. Traditional force fields address this by ensuring equivalent orderings of atom types receive the same parameter value.<sup>1</sup>

For neural embeddings, the invariance of valence terms to these atom ordering symmetries must be considered while searching for expressive fixed-length vector representations to feed into a subsequent parameter prediction network stage. Inspired by Janossy pooling [58], we enumerate the the relevant equivalent atom permutations to derive bond, angle, and torsion embeddings  $h_r, h_\theta, h_\phi$  that respect these symmetries from atom embeddings  $h_v$ ,

$$h_{r_{ij}} = \text{NN}_r([h_{v_i} : h_{v_j}]) + \text{NN}_r([h_{v_j} : h_{v_i}]); \quad (17)$$

$$h_{\theta_{ijk}} = \text{NN}_\theta([h_{v_i} : h_{v_j} : h_{v_k}]) + \text{NN}_\theta([h_{v_k} : h_{v_j} : h_{v_i}]); \quad (18)$$

$$h_{\phi_{ijkl\text{proper}}} = \text{NN}_{\phi_{\text{proper}}}([h_{v_i} : h_{v_j} : h_{v_k} : h_{v_l}]) + \text{NN}_\phi([h_{v_l} : h_{v_k} : h_{v_j} : h_{v_i}]); \quad (19)$$

$$h_{\phi_{ijkl\text{improper}}} = \text{NN}_{\phi_{\text{improper}}}([h_{v_i} : h_{v_j} : h_{v_k} : h_{v_l}]) + \text{NN}_\phi([h_{v_k} : h_{v_j} : h_{v_l} : h_{v_i}]) + \text{NN}_{\phi_{\text{improper}}}([h_{v_l} : h_{v_j} : h_{v_i} : h_{v_k}]), \quad (20)$$

where columns  $(\cdot : \cdot)$  denote concatenation<sup>2</sup>. As such, the order invariance is evident, i.e.,  $h_{r_{ij}} = h_{r_{ji}}$ ,  $h_{\theta_{ijk}} = h_{\theta_{kji}}$ , and  $h_{\phi_{ijkl}} = h_{\phi_{lkji}}$ <sup>3</sup>.

<sup>1</sup>Traditional force fields group bonds, angles, and torsions simply by their composing ordered groups of atoms. For instance, the first bond type in GAFF 1.81 [53] is defined by the types `hw-ow` <https://github.com/openmm/openmmforcefields/blob/0.9.0/amber/gaff/dat/gaff-1.81.dat#L87>, which is equivalent to `ow-hw` due to mirror symmetry in identifying bonds. Angles and torsions have similar symmetries that must to be accounted for when enumerating the atoms or matching valence types.

<sup>2</sup>Here, we use the threefold improper formulation used by the Open Force Field "Parsley" generation force fields, which avoids the ambiguity associated with selecting a single arbitrary improper torsion from a set of four atoms involved in the torsion [57].

<sup>3</sup>In SI Section 20, we prove that this form is sufficiently expressive to assign unique valence types.

### 2.3 Stage 3: Neural parametrization of atoms, bonds, angles, and torsions replaces tabulated parameter assignment

In the final stage, feed-forward neural networks learn the mapping from these symmetry-invariant atom, bond, angle, and torsion encodings to MM parameters  $\Phi_{\text{FF}}$  that reflect the specific chemical environments appropriate for these terms. Each distinct parameter class (such as atom parameters, bond parameters, angle parameters, and torsion parameters) is assigned by a separate neural network, making this stage fully modular:

$$\{\epsilon_v, \sigma_v\} = \text{NN}_{v_{\text{readout}}}(h_v) \quad \text{atom parameters} \quad (21)$$

$$\{k_r, b_r\} = \text{NN}_{r_{\text{readout}}}(h_r) \quad \text{bond parameters} \quad (22)$$

$$\{k_\theta, b_\theta\} = \text{NN}_{\theta_{\text{readout}}}(h_\theta) \quad \text{angle parameters} \quad (23)$$

$$\{k_\phi\} = \text{NN}_{\phi_{\text{readout}}}(h_\phi) \quad \text{torsion parameters} \quad (24)$$

This stage is analogous to the final table lookup step in traditional force field construction, but with significant added flexibility arising from the continuous embedding that captures the chemical environment specific to the potential energy term being assigned. Note that, in our implementation, we do not produce LJ parameters but use that from legacy force fields (Open Force Field 1.2.0 [59] in this paper) since those are fit to other parameters namely physical properties. Moreover, we do not fit equilibrium bonds and angles but use a mixture of linear basis to represent harmonic energies which can be translate back to the original functional form (See Section 2.4.1). Similarly, we do not fit phases and periodicities of torsions but use 0 as phases and 0  $\tilde{b}$  periodicities with parametrized  $K$  which is not constrained and could be negative. As a result, intelligent interpolation between relevant chemical environments seen during training is possible, producing more nuanced varieties of parameters than either traditional atom typing or direct chemical perception, capable of capturing subtle effects arising from fractional bond order perturbation [38]. Due to the modularity of this stage, it is easy to add new modules or swap out existing ones to explore other force field functional forms, such as alternative vdW interactions [60]; pair-specific Lennard-Jones interaction parameters [51]; point polarizabilities for instantaneous dipole [61], Drude oscillator [62], or Gaussian charge [63] polarizability models; class II valence couplings [64–66]; charge transfer [39]; or other potential energy terms of interest.

### 2.4 Training and inference

While traditional force fields based on discrete atom types are only differentiable with respect to the molecular mechanics parameters they assign, our model is fully differentiable in *all* model parameters  $\Phi_{\text{NN}}$  that govern both the assignment of continuous atom embeddings  $h_v$  (which replace discrete atom types) and subsequent assignment of MM parameters  $\Phi_{\text{FF}}$ . We can therefore use gradient-based optimization to tune all of these parameters to fit arbitrary differentiable target functions, such as energies and forces of snapshots of molecules, equilibrium physical property measurements, fluctuation properties, or experimentally measured free energy differences. In this way, straightforward gradient-based optimization simultaneously learns the continuous equivalent of atom typing simultaneous with parameter assignment strategies, effectively solving the intractable traditional force field parameterization problem of mixed continuous-discrete optimization by replacing it with a fully continuous optimization problem.

#### 2.4.1 A linear basis facilitates bond and angle parameter optimization

The harmonic functional form (Equation 6),

$$u(x; K, b) = \frac{K}{2}(x - b)^2, \quad (25)$$

is frequently used in MM potentials for modeling bond and angle energies. Although one can directly optimize force constants  $K$  and equilibrium bond or angle values  $b$ , this empirically result in significant difficulties in training (Figure 2). This can be seen through the loss function and its gradient for a simple toy model

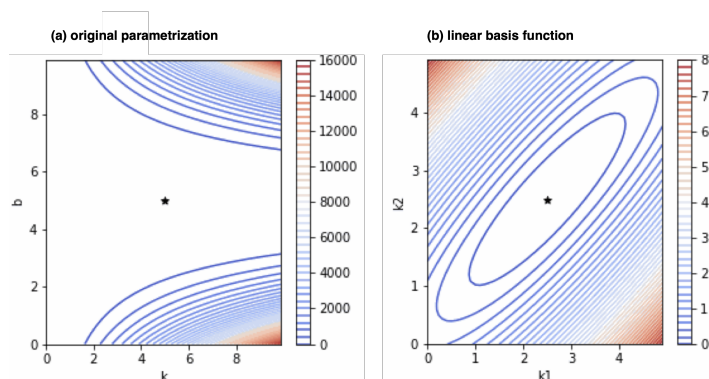


**Figure 2. Linear basis parameterization of bonds and angles facilitates robust optimization.** A one-dimensional harmonic oscillator system ( $u = \frac{K_0}{2}(x - b_0)^2$ ) was simulated with  $K_0 = 5$ ,  $b_0 = 5$  as reference parameters. Training set conformations  $x$  were sampled from a uniform distribution with  $x \sim \text{Uniform}(4, 6)$ . The loss function (squared energy error) as a function of original MM parameters ( $K$ ,  $b$ ) shown in (a) is clearly more difficult to optimize due to the large difference in gradient magnitudes between  $K$  and  $b$  parameters, while the linear basis parametrization (Section 2.4.1) showing the loss as a function of transformed ( $K_1$ ,  $K_2$ ) in (b) is much simpler to optimize.

consisting of a single bond and reference parameters ( $K_0$ ,  $b_0$ ):

$$L(K, b) = \sum_{n=1}^N [u(x_n; K, b) - u(x_n; K_0, b_0)]^2 \quad (26)$$

$$= \sum_{n=1}^N \left[ \frac{K}{2}(x_n - b)^2 - \frac{K_0}{2}(x_n - b_0)^2 \right]^2 \quad (27)$$

Qualitatively, the loss function landscape for  $K$  around  $K_0$  is relatively flat, while it is steeply varying for  $b$  around  $b_0$ , frustrating efficient optimization; Figure 2a demonstrates this for a simple toy system. To circumvent this issue, we use the approach described by Vanommeslaeghe et al. [67] and translate the harmonic functional form Equation 25 in which ( $K$ ,  $b_0$ ) are optimized instead into a linear combination ( $K_1$ ,  $K_2$ ) of basis functions is optimized instead:

$$u(x; K_1, K_2) = \underbrace{\frac{K_1}{2}(x - b_1)^2 + \frac{K_2}{2}(x - b_2)^2}_{\text{linear combination of basis}} + \underbrace{\left( -K_1 b_1^2 - K_2 b_2^2 + \frac{(K_1 b_1 + K_2 b_2)^2}{K_1 + K_2} \right)}_{x\text{-independent constant}} \quad (28)$$

where  $b_1$  and  $b_2$  are two positive constants chosen to be smaller and larger than any possible valid bond or angle—they must satisfying  $b_1 < x < b_2$  for  $\forall x$  that might be observed. Here, Stage III of the Espaloma pipeline would predict  $K_1$ ,  $K_2$ , which would be used to compute the MM parameters ( $K$ ,  $b$ ) via

$$K = K_1 + K_2 \quad (29)$$

$$b = \frac{K_1 b_1 + K_2 b_2}{K_1 + K_2} \quad (30)$$

When training to fit energies, our loss function subtracts the mean from the training set energies and predicted energies for each molecule to remove the arbitrary offset constant introduced by this transformation of variables.

#### 2.4.2 Training by potential energies

Given a training set of molecules  $\{\mathcal{G}_m\}$ ,  $m = 1, \dots, M$ , with corresponding  $n = 1, \dots, N_m$  conformational snapshots  $\mathbf{x}_{m,n} \in \mathbf{R}^{(|\mathcal{G}_m| \times 3)}$  for each molecule  $m$ , and reference potential energies  $\{U_{\text{ref}}(x_{m,n}; \mathcal{G}_m)\}$ , the model parameters  $\Phi_{\text{NN}}$  can be optimized to minimize a measure of deviation between the reference energies and model energies given by the composed force field  $\Phi_{\text{FF},\theta}$ . For example, a squared loss function can be used to quadratically penalize deviations:

$$\mathcal{L}(\Phi_{\text{NN}}) = \sum_{m=1}^M \sum_{n=1}^{N_m} w_{m,n} \left[ U_{\text{ref}}(x_{m,n}; \mathcal{G}_m) - U_{\Phi_{\text{FF},\theta}}(\mathbf{x}_{m,n}; \mathcal{G}_m) \right]^2 \quad (31)$$

In this work, we took the weights  $w_{m,n} = 1$ , but more sophisticated weighting schemes can be used to emphasize low-energy snapshots where MM potentials are intended to be more accurate when fitting to quantum chemical datasets, as in ForceBalance [68, 69]. In a Bayesian context, the loss function in Eq. ?? would correspond to the negative log likelihood for a normal error model. Other loss or likelihood function forms may also be useful in ensuring a minority of molecules or geometries for which the MM functional form poorly reproduces quantum chemical energetics do not dominate the fit.

Additional terms can be added to the loss function to regularize the choice of parameters, such as penalizing unphysical choices (such as unphysical magnitudes or parameter regions) or to provide more useful models (such as penalizing bond vibrations with effective periods that are so short they would require extremely small timesteps).

When fitting to quantum chemical energies, an additive offset for each molecule  $m$  corresponding to the heat of formation generally cannot be accounted for using standard MM functional forms. To address this, we subtract the per-molecule mean potential energy for both predicted MM and reference quantum chemical energies in formulating the loss function, with the goal of ensuring that relative conformational energetics are accurately approximated even if the heat of formation cannot be computed.

### 2.4.3 Other differentiable objectives

In quantum chemical calculations, nuclear potential energy gradients are often available at very low cost once the wavefunction has been solved to compute the energy. To exploit the rich information available in these gradients [70–73]  $\nabla_x U$ , it is possible to incorporate both energies and gradients into the loss function, with automatic differentiation used to compute partial derivatives of the Espaloma energy function in terms of both coordinates and parameters. Additional terms penalizing deviations in more complex quantum chemical properties, such as polarizabilities or vibrational frequencies, could also be incorporated [68, 69]. In this work, however, we found that incorporation of gradient information does not significantly enhance the performance of the model. We leave this topic to future study.

In addition to incorporating configuration-dependent properties, if the goal is to build a complete molecular mechanics force field to model entire physical systems in the condensed phase, additional terms could be added to the objective function to quantify the deviation in physical properties, such as densities, dielectric constants, and enthalpies of vaporization [68, 69, 74–77], or even experimental transfer free energies.

### 2.4.4 Assigning Espaloma parameters to molecules

In contrast with many quantum machine learning (QML) force fields that use a neural model to compute the energy and gradient for every configuration [10, 78, 79], **Espaloma** uses a neural model to assign molecular mechanics parameters *once* at the beginning of a simulation, using only the chemical information about all components in a system. Once generated, the MM parameters  $\Phi_{\text{ff}}$  for the system can be seamlessly ported to molecular mechanics packages that can exploit accelerated hardware [2, 16–18] to achieve high accuracy for individual systems at the same speed as traditional force fields.

---

```
# define or load a molecule of interest via the Open Force Field toolkit
from openff.toolkit.topology import Molecule
molecule = Molecule.from_smiles("CN1C=NC2=C1C(=O)N(C(=O)N2C)C")

# create an Espaloma Graph object to represent the molecule of interest
import espaloma as esp
molecule_graph = esp.Graph(molecule)

# apply a trained espaloma model to assign parameters
espaloma_model = torch.load("espaloma_model.pt")
espaloma_model(molecule_graph.heterograph)

# create an OpenMM System for the specified molecule
openmm_system = esp.graphs.deploy.openmm_system_from_graph(molecule_graph)
```

---

**Listing 2.** Using a trained Espaloma model to assign parameters to a small molecule.

### 3 Graph neural networks can learn to reproduce human-defined legacy atom types with high accuracy

Traditional molecular mechanics force field parameter assignment schemes such as Antechamber/GAFF [52, 53] or CGenFF [80, 81] use attributes of atoms and their neighbors (such as atomic number, hybridization, and aromaticity) to assign discrete atom types, subsequently assigning atom, bond, angle, and torsion parameters to specific combinations of these discrete types. Traditionally, these approaches have relied on human physical chemistry intuition to craft these distinct atom type classes [21]. We wondered whether graph neural networks of the sort used in Espaloma Stage 1 (continuous atom embedding) were sufficiently expressive to capture these human-specified atom types by asking whether they could reproduce reproduce legacy (human-designed) atom types for a widely popular<sup>4</sup> general small organic molecule force field, GAFF 1.81 [52, 53].

Because Espaloma uses continuous atom embeddings, to address this question, we introduce an additional feedforward layer to compute a predicted identity vector from the latent embedding of atoms  $h_v$  produced by the Stage 1 output, described in Section 2.1.1. The loss on training data is then minimized when the cross-entropy loss between predicted and reference types is minimized. Note that this discrete type assignment layer is only used to address the question of how well the continuous embeddings approximate discrete types, and is not used in subsequent experiments that utilize the standard Espaloma architecture (Figure 1).

We use a subset of ZINC [82] provided with parm@frosst to validate atom typing implementations [83] (7529 molecules, partitioned 80:10:10 into training:validation:test sets) for this experiment. Reference GAFF 1.81 [53] atom types are assigned using Antechamber [53] from AmberTools and are used for training and testing.

The test set performance is reported in Figure 3, where the overall accuracy between reference legacy types and learned types is very high—98.31%<sup>98.63%</sup><sub>97.94%</sub>. In analyzing the infrequent failures, we find the model assigns atom types that correspond to the reference type more often when the atom type appears more frequently in the training data, whereas the discrepancies occur in assigning rare types and types whose definitions follow a more sophisticated (but chemically arbitrary) logic. For instance, one of the most frequent confusions is the misassignment of `ca` (sp<sup>2</sup> carbon in pure aromatic systems) to `cp` (head sp<sup>2</sup> carbon that connects two rings in biphenyl systems, occurring in only 0.6% of the dataset). The relative ambiguity of the various types that are most frequently confused is suggestive that the graph net makes human-like errors in perceiving subtle differences between distinct chemical environments.

### 4 Espaloma can learn molecular mechanics force fields from potential energies

Having established that graph neural networks have the capacity to learn to reproduce legacy atom types describing distinct chemical environments, we ask whether Espaloma is capable of learning to reproduce traditional molecular mechanics (MM) force fields assigned via standard atom typing schemes. In addition to quantifying how well a force field can be learned when the exact parameters of the model being learned are known, being able to accurately learn existing MM force fields would have numerous applications, including replacing legacy non-portable parameter assignment codes with modern portable machine learning frameworks, learning to generalize to new molecules that contain familiar chemical environments, and permitting simplified parameter assignment for complex, heterogeneous systems involving post-translational modifications, covalent ligands, or heterogeneous combinations of biopolymers and small molecules.

To assess how well Espaloma can learn to reproduce an MM force field from a limited amount of data, we selected a chemical dataset of limited complexity—PhAlkEthOH [85, 86]—which consists of 7408 linear and cyclic molecules containing phenyl rings, small alkanes, ethers, and alcohols composed of only the elements carbon, oxygen, and hydrogen. We generated a set of conformational snapshots for each molecule using short high-temperature molecular dynamics simulations at 300 K initiated from multiple conformations to ensure adequate sampling of conformers. The AlkEthOH dataset was randomly partitioned (by molecules) into 80% training, 10% validation, and 10% test molecules, with 100 snapshots/molecule, and an Espaloma

<sup>4</sup>GAFF [52] has been cited over 11,913 times as of 4 Sep 2021.

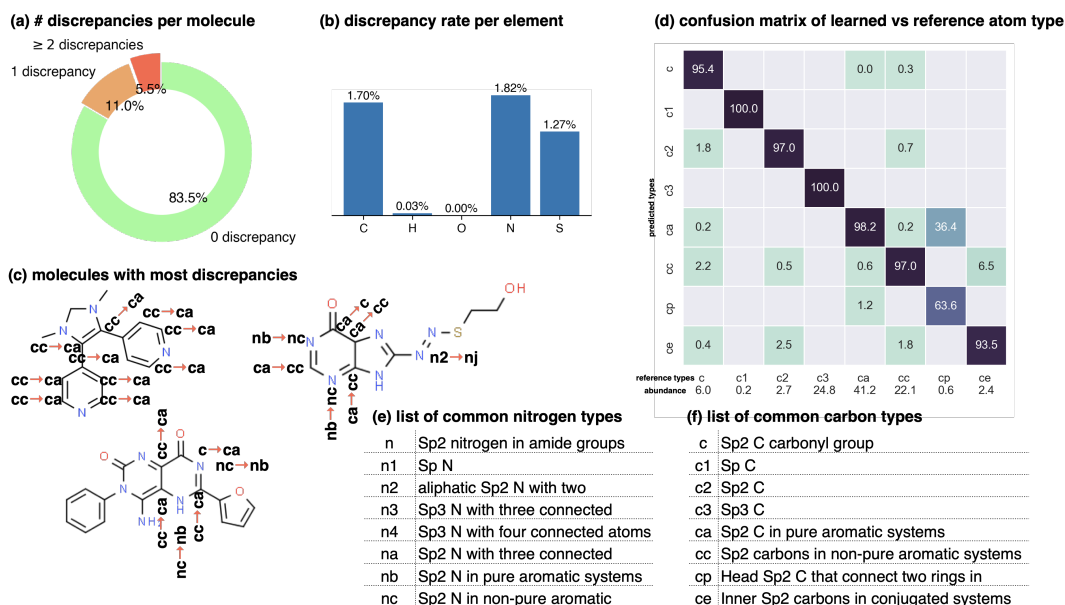


**Figure 3. Graph neural networks can reproduce legacy atom types with high accuracy.** The Stage 1 graph neural network of Espaloma chained to a discrete atom type readout was fit to GAFF 1.81 atom types [52, 53] on a subset of ZINC [82] distributed with parmFrosst [83] as a validation set (Section 3). The 7529 molecules in this set were partitioned 80:10:10 into training:test:validation sets for this experiment. The overall test set accuracy was 99.07%<sup>99.22%</sup>, with 1000 bootstrap replicates used to estimate the confidence intervals arising from finite test set size effects. (a) The distribution of the number of atom type discrepancies on the test set demonstrates that only a minority of atoms are incorrectly typed. (b) The error rate per element is primarily concentrated within carbon, nitrogen, and sulfur types. (c) Examining atom type failures in detail on molecules with the largest numbers of discrepancies shows that the atom types are easily confused by a human, since they represent qualities that are difficult to precisely define. (d) The distribution of predicted atom types for each reference atom type for carbon types are shown; on-diagonal values indicate agreement. The percentages annotated under x-axis denote the relative abundance within the test set. Only the common carbon types are included in the confusion matrix here; for full confusion matrix across all atom types, see SI Figure 11. (e) A list of common nitrogen types in GAFF-1.81 [84]. (f) A list of common carbon types in GAFF-1.81 [84].

model was trained with early stopping via monitoring for a decrease in accuracy in the validation set. The performance of the resulting model is reported in Table 4.

The overall root mean squared error (RMSE) on bond and angle energy is less than 0.05 kcal/mol. Note that, as judged by correlation coefficient ( $R^2$ ) and mean absolute percentage error (MAPE), the equilibrium length and angle achieved a better performance compared to force constants.

**Ablation study: the role of energy centering, the inclusion of torsion energies, and the inclusion of small rings in datasets in the performance of MM fitting.**

We closely examined several choices which appear to have significant impact on the ability to produce high-quality generalizable models for the task of learning an MM potential: Concretely, we conduct an ablation study (Table 1) where we repeat the experiment shown in Figure 4 considering several variations of these choices:

**Small rings (R):** We consider whether molecules with small (3- or 4-membered) rings are included in the dataset, since these molecules assume geometries have near-degeneracies in equilibrium angles (Figure 6).

**Energy centering (C):** We consider the role of energy centering in the loss function, where the average potential energy over all conformations for each molecule is subtracted for both reference and predicted energies in the loss function, such that only relative conformational energy errors are penalized. We evaluate the error both with and without centering. **Torsion energies (T):** We also consider whether torsion energies are included as well, since recovery of torsion profiles can be challenging due to both the near-degeneracy of parameters and phases. Notably, while MM force fields generally specify a minimal set of a few torsion periodicities with phases of 0 or  $\pi$  explicitly specified, we use a formulation where all periodic-

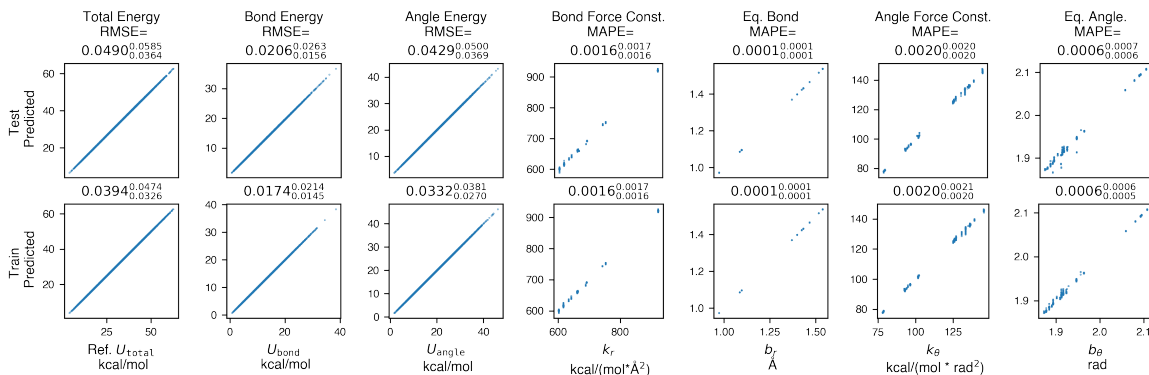


**Figure 4. Espaloma accurately learns molecular mechanics parameters when fit to snapshot energies from a molecular mechanics force field.** In this experiment, Espaloma was used to fit molecular mechanics (GAFF 1.81) potential energies of snapshots generated from short molecular dynamics (MD) simulations initiated from multiple conformers of molecules from the PhAlkEthOH dataset, which uses only the elements carbon, oxygen, and hydrogen [86]. The dataset contains 7408 molecules, and was partitioned by molecules 80:10:10 into train:validate:test sets. We excluded torsion energies from the loss function, and three- and four-membered rings in the dataset; for a detailed study on the roles of these two factors, see Table 1. Statistics quoted above the plots provide the root mean squared error (RMSE) between reference and predicted MM energies, and mean absolute percentage error (MAPE) (in fractional form) between reference and predicted force field parameters. The sub- and superscripts report the the 95% confidence interval of each statistics estimated from 1000 bootstrapped replicates over molecules in the test set. Energy terms have kcal/mol units whereas the units of force field parameters does not affect statistics reported here. Force field parameters ( $\Phi_{FF}$ ):  $K_r$ : bond force constant;  $b_r$ : equilibrium bond length;  $K_\theta$ : angle force constant;  $b_\theta$ : equilibrium angle value. Torsion parameters are not shown because of the potential degeneracy of fit given that all periodicities up to  $n = 6$  are learned by Espaloma.

R C T Part	$U_{total}$	$U_{bond}$			$U_{torsion}$				$k_r$	$b_r$	$k_\theta$	$b_\theta$	
		RMSE (kcal/mol)			Centered RMSE (kcal/mol)								MAPE
000	test	0.8723 <sup>0.9334</sup> <sub>0.8139</sub>	1.2725 <sup>1.4465</sup> <sub>1.0575</sub>	1.2291 <sup>1.4102</sup> <sub>0.9563</sub>									
	train	0.9183 <sup>0.9889</sup> <sub>0.8343</sub>	1.3159 <sup>1.5514</sup> <sub>1.0655</sub>	1.2844 <sup>1.5360</sup> <sub>1.0052</sub>									
001	test	4.4033 <sup>4.6173</sup> <sub>4.1317</sub>	13.7163 <sup>14.5515</sup> <sub>12.9510</sub>	7.9210 <sup>8.4048</sup> <sub>7.3953</sub>	0.0363 <sup>0.0384</sup> <sub>0.0345</sub>	3.5238 <sup>3.6590</sup> <sub>3.3844</sub>	3.0956 <sup>3.2187</sup> <sub>2.9908</sub>	1.7086 <sup>1.7619</sup> <sub>1.6367</sub>	0.0015 <sup>0.0017</sup> <sub>0.0014</sub>	1.0000 <sup>1.0000</sup> <sub>1.0000</sub>	0.0720 <sup>0.0740</sup> <sub>0.0701</sub>	0.4734 <sup>0.4763</sup> <sub>0.4712</sub>	0.0136 <sup>0.0138</sup> <sub>0.0134</sub>
	train	4.2372 <sup>4.5129</sup> <sub>3.9854</sub>	13.2693 <sup>14.2219</sup> <sub>12.1669</sub>	8.0467 <sup>8.6800</sup> <sub>7.4667</sub>	0.0353 <sup>0.0379</sup> <sub>0.0330</sub>	3.5041 <sup>3.6277</sup> <sub>3.3614</sub>	3.0243 <sup>3.1645</sup> <sub>2.9115</sub>	1.7425 <sup>1.8182</sup> <sub>1.6659</sub>	0.0016 <sup>0.0017</sup> <sub>0.0014</sub>	1.0000 <sup>1.0000</sup> <sub>1.0000</sub>	0.0705 <sup>0.0720</sup> <sub>0.0686</sub>	0.4803 <sup>0.4831</sup> <sub>0.4778</sub>	0.0137 <sup>0.0139</sup> <sub>0.0135</sub>
010*	test	0.0490 <sup>0.0585</sup> <sub>0.0369</sub>	0.0206 <sup>0.0262</sup> <sub>0.0158</sub>	0.0429 <sup>0.0497</sup> <sub>0.0362</sub>		0.0175 <sup>0.0187</sup> <sub>0.0160</sub>	0.0130 <sup>0.0140</sup> <sub>0.0121</sub>	0.0117 <sup>0.0127</sup> <sub>0.0105</sub>	0.0016 <sup>0.0017</sup> <sub>0.0016</sub>	0.0001 <sup>0.0001</sup> <sub>0.0001</sub>	0.0020 <sup>0.0020</sup> <sub>0.0020</sub>	0.0006 <sup>0.0006</sup> <sub>0.0006</sub>	0.0006 <sup>0.0006</sup> <sub>0.0006</sub>
	train	0.0394 <sup>0.0478</sup> <sub>0.0315</sub>	0.0174 <sup>0.0206</sup> <sub>0.0142</sub>	0.0332 <sup>0.0394</sup> <sub>0.0271</sub>		0.0169 <sup>0.0178</sup> <sub>0.0160</sub>	0.0120 <sup>0.0135</sup> <sub>0.0118</sub>	0.0113 <sup>0.0121</sup> <sub>0.0103</sub>	0.0016 <sup>0.0016</sup> <sub>0.0016</sub>	0.0001 <sup>0.0001</sup> <sub>0.0001</sub>	0.0020 <sup>0.0021</sup> <sub>0.0020</sub>	0.0006 <sup>0.0006</sup> <sub>0.0006</sub>	0.0006 <sup>0.0006</sup> <sub>0.0006</sub>
011	test	11.0688 <sup>12.8267</sup> <sub>8.8832</sub>	0.0240 <sup>0.0284</sup> <sub>0.0204</sub>	0.1801 <sup>0.2122</sup> <sub>0.1535</sub>	0.0174 <sup>0.0203</sup> <sub>0.0145</sub>	0.0346 <sup>0.0369</sup> <sub>0.0324</sub>	0.0166 <sup>0.0180</sup> <sub>0.0157</sub>	0.0270 <sup>0.0307</sup> <sub>0.0226</sub>	0.0001 <sup>0.0001</sup> <sub>0.0001</sub>	0.0020 <sup>0.0021</sup> <sub>0.0020</sub>	0.0001 <sup>0.0001</sup> <sub>0.0001</sub>	0.0020 <sup>0.0021</sup> <sub>0.0020</sub>	0.0006 <sup>0.0006</sup> <sub>0.0006</sub>
	train	11.7819 <sup>14.0593</sup> <sub>9.4086</sub>	0.0190 <sup>0.0203</sup> <sub>0.0179</sub>	0.1899 <sup>0.2335</sup> <sub>0.1545</sub>	0.0185 <sup>0.0216</sup> <sub>0.0152</sub>	0.0335 <sup>0.0357</sup> <sub>0.0302</sub>	0.0161 <sup>0.0173</sup> <sub>0.0150</sub>	0.0284 <sup>0.0321</sup> <sub>0.0238</sub>	0.0001 <sup>0.0001</sup> <sub>0.0001</sub>	0.0020 <sup>0.0021</sup> <sub>0.0020</sub>	0.0001 <sup>0.0001</sup> <sub>0.0001</sub>	0.0020 <sup>0.0021</sup> <sub>0.0020</sub>	0.0006 <sup>0.0006</sup> <sub>0.0006</sub>
100	test	0.6237 <sup>0.7049</sup> <sub>0.5459</sub>	0.5224 <sup>0.5707</sup> <sub>0.4774</sub>	0.6660 <sup>0.7498</sup> <sub>0.5843</sub>		0.4970 <sup>0.5526</sup> <sub>0.4483</sub>	0.3380 <sup>0.3614</sup> <sub>0.3176</sub>	0.4654 <sup>0.5205</sup> <sub>0.4084</sub>	0.0016 <sup>0.0017</sup> <sub>0.0016</sub>	0.0466 <sup>0.0479</sup> <sub>0.0459</sub>	0.0012 <sup>0.0013</sup> <sub>0.0012</sub>	0.0645 <sup>0.0662</sup> <sub>0.0624</sub>	0.0111 <sup>0.0117</sup> <sub>0.0107</sub>
	train	0.6615 <sup>0.7584</sup> <sub>0.5706</sub>	0.6199 <sup>0.6905</sup> <sub>0.6107</sub>	0.6939 <sup>0.7702</sup> <sub>0.6107</sub>		0.5693 <sup>0.6494</sup> <sub>0.4963</sub>	0.3916 <sup>0.4304</sup> <sub>0.3473</sub>	0.5293 <sup>0.6160</sup> <sub>0.4489</sub>	0.0016 <sup>0.0017</sup> <sub>0.0016</sub>	0.0482 <sup>0.0493</sup> <sub>0.0473</sub>	0.0013 <sup>0.0013</sup> <sub>0.0013</sub>	0.0659 <sup>0.0677</sup> <sub>0.0637</sub>	0.0112 <sup>0.0117</sup> <sub>0.0108</sub>
101	test	4.7719 <sup>4.9088</sup> <sub>4.6354</sub>	9.5963 <sup>9.9684</sup> <sub>9.1500</sub>	23.1972 <sup>24.2192</sup> <sub>22.2322</sub>	0.0501 <sup>0.0519</sup> <sub>0.0480</sub>	4.3643 <sup>4.4498</sup> <sub>4.2279</sub>	2.6994 <sup>2.7756</sup> <sub>2.6075</sub>	3.6263 <sup>3.6948</sup> <sub>3.5347</sub>	0.0020 <sup>0.0022</sup> <sub>0.0019</sub>	0.8410 <sup>0.8440</sup> <sub>0.8386</sub>	0.0263 <sup>0.0267</sup> <sub>0.0259</sub>	1.0000 <sup>1.0000</sup> <sub>1.0000</sub>	0.9287 <sup>0.9294</sup> <sub>0.9282</sub>
	train	4.8043 <sup>4.9617</sup> <sub>4.6731</sub>	9.3807 <sup>9.8568</sup> <sub>8.8160</sub>	23.2491 <sup>24.1563</sup> <sub>22.4420</sub>	0.0495 <sup>0.0514</sup> <sub>0.0481</sub>	4.4050 <sup>4.5169</sup> <sub>4.2726</sub>	2.6971 <sup>2.7786</sup> <sub>2.6393</sub>	3.5734 <sup>3.6850</sup> <sub>3.4918</sub>	0.0019 <sup>0.0021</sup> <sub>0.0018</sub>	0.8404 <sup>0.8428</sup> <sub>0.8371</sub>	0.0267 <sup>0.0272</sup> <sub>0.0263</sub>	1.0000 <sup>1.0000</sup> <sub>1.0000</sub>	0.9281 <sup>0.9288</sup> <sub>0.9275</sub>
110	test	89.0006 <sup>102.2105</sup> <sub>80.4894</sub>	0.0384 <sup>0.0440</sup> <sub>0.0339</sub>	88.9808 <sup>107.0304</sup> <sub>64.5673</sub>		0.0223 <sup>0.0257</sup> <sub>0.0200</sub>	0.0246 <sup>0.0269</sup> <sub>0.0221</sub>	0.0278 <sup>0.0310</sup> <sub>0.0247</sub>	0.0018 <sup>0.0019</sup> <sub>0.0018</sub>	0.0018 <sup>0.0019</sup> <sub>0.0018</sub>	0.0033 <sup>0.0035</sup> <sub>0.0032</sub>	0.0074 <sup>0.0089</sup> <sub>0.0064</sub>	
	train	79.6927 <sup>99.1904</sup> <sub>62.4512</sub>	0.1155 <sup>0.1224</sup> <sub>0.0351</sub>	79.6589 <sup>98.9583</sup> <sub>69.2236</sub>		0.0209 <sup>0.0205</sup> <sub>0.0203</sub>	0.0811 <sup>0.0821</sup> <sub>0.0814</sub>	0.0814 <sup>0.0814</sup> <sub>0.0814</sub>	0.0016 <sup>0.0017</sup> <sub>0.0016</sub>	0.0016 <sup>0.0017</sup> <sub>0.0016</sub>	0.0001 <sup>0.0001</sup> <sub>0.0001</sub>	0.0031 <sup>0.0032</sup> <sub>0.0031</sub>	0.0066 <sup>0.0066</sup> <sub>0.0066</sub>
111	test	99.6155 <sup>118.2089</sup> <sub>75.0240</sub>	0.0586 <sup>0.0661</sup> <sub>0.0520</sub>	91.7758 <sup>115.4096</sup> <sub>71.2381</sub>	0.0245 <sup>0.0270</sup> <sub>0.0222</sub>	0.0297 <sup>0.0352</sup> <sub>0.0236</sub>	0.032 <sup>0.0371</sup> <sub>0.0282</sub>	0.0438 <sup>0.0492</sup> <sub>0.0398</sub>	0.0000 <sup>0.0001</sup> <sub>0.0000</sub>	0.0011 <sup>0.0011</sup> <sub>0.0011</sub>	0.0001 <sup>0.0001</sup> <sub>0.0001</sub>	0.0034 <sup>0.0036</sup> <sub>0.0032</sub>	0.0077 <sup>0.0087</sup> <sub>0.0066</sub>
	train	90.1890 <sup>113.6430</sup> <sub>70.8691</sub>	0.1682 <sup>0.2789</sup> <sub>0.0543</sub>	81.6664 <sup>108.1073</sup> <sub>64.1198</sub>	0.0264 <sup>0.0290</sup> <sub>0.0236</sub>	0.0279 <sup>0.0299</sup> <sub>0.0258</sub>	0.1011 <sup>0.1693</sup> <sub>0.0311</sub>	0.1043 <sup>0.1679</sup> <sub>0.0440</sub>	0.0001 <sup>0.0001</sup> <sub>0.0001</sub>	0.0017 <sup>0.0018</sup> <sub>0.0017</sub>	0.0001 <sup>0.0001</sup> <sub>0.0001</sub>	0.0033 <sup>0.0035</sup> <sub>0.0031</sub>	0.0066 <sup>0.0075</sup> <sub>0.0055</sub>

**Table 1. Best performance of MM fitting on PhAlkEthOH dataset only when centering is deployed and torsion energy and small rings are excluded.** A comparison of Espaloma MM fitting experiments on PhAlkEthOH dataset with/without fitting torsions, centering energies, and including three- and four-membered rings. The **R C T** column summarizes the experimental conditions: **R** indicates whether small (3- and 4-membered) rings were included in the dataset (1 small rings included, 0 excluded); **C** indicates whether the potential energies for sampled snapshots of each molecule were centered by subtracting off the mean energy for that molecule in the loss function (1 centered, 0 uncentered); **T** indicates whether torsion energies were included in the fitting (1 included, 0 excluded). The rest of the experimental setting is identical with Figure 4. Force field parameters ( $\Phi_{FF}$ ):  $K_r$ : bond force constant;  $b_r$ : equilibrium bond length;  $K_\theta$ : angle force constant;  $b_\theta$ : equilibrium angle value. The root mean squared error (RMSE) and correlation coefficient ( $R^2$ ) between reference and predicted MM energies, as well as mean absolute percentage error (MAPE) (as a fraction rather than a percentage, i.e. not multiplied by 100), and correlation coefficient ( $R^2$ ) between reference and predicted force field parameters. The sub- and superscripts report the the 95% confidence interval of each statistics estimated from 1000 bootstrapped replicates on the molecule set. \*: Same experiment as Figure 4.

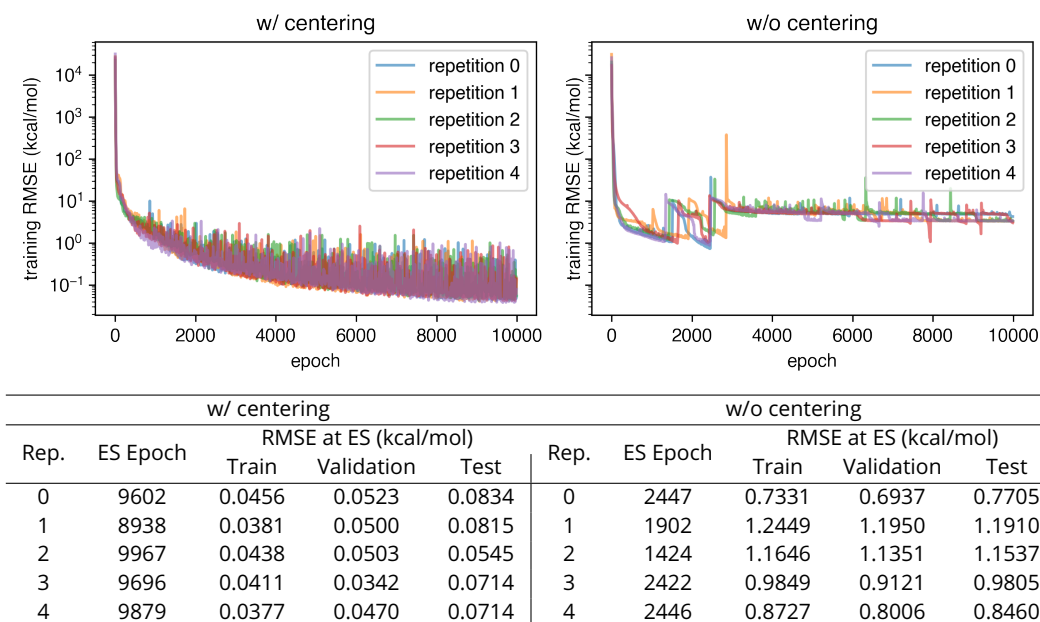


**Figure 5. Espaloma models are difficult to train, especially when attempting to fit to absolute (rather than relative) conformation energies.** We compare the training trajectory of Espaloma without torsion energy on PhAlkEthOH dataset excluding three- and four-membered rings with and without centering (experiments 010 and 000 in Table 1). Example training trajectories with the same setting as Figure 4. Various repetitions are plotted in different colors.

ities  $n = 1, 2, \dots, 6$  are always fit and the sign of the torsion  $K$  parameter indicates whether the phase is 0 ( $K > 0$ ) or  $\pi$  ( $K < 0$ ).

Experiments for all combinations of these choices are shown in Table 1.

We summarize our findings as follow: First of all, best performance is only achieved when we center the predicted and reference energies in the loss function used in training, effectively training to fit only relative energies, suggesting this makes robust optimization easier. The rationalization could be found in Section 2.4.1. We also examined the training trajectory of Espaloma on this MM fitting task with and without the centering of predicted and reference energies (Figure 5) and noticed that centering alleviates, but not completely remedies the training difficulties of Espaloma models.

Secondly, the inclusion of torsion energies deteriorates performance, especially if measured by uncentered RMSE. This could be attributed to the fact that we use a slightly different functional form to express torsion energies than reference legacy force fields.

Lastly, with energy centering, including three- and four-membered rings in our training set results in very large uncentered RMSE without drastically changing the centered RMSE (relative conformational energy errors). We study this effect in detail in the next section.

#### Case Study: Parametrization of Cyclopropane

We use the model trained on PhAlkEthOH dataset with the inclusion of small rings but without torsion energies (experiment 110 in Table 1) and apply this model to cyclopropane (SMILES: C1CC1) As shown in (b) in Figure 6, when trained with centered energy loss function (Section 31), Espaloma assigned equilibrium angle value  $\theta_0 \approx 122.1^\circ$  to the CCC angle in cyclopropane while the equilibrium angle is  $60^\circ$  in the reference GAFF-1.81 force field. With a shift in angle force constant, while this would drastically change the energies of individual CCC angles, the sum of energies of the three CCC angles (whose angle values would sum up to  $180^\circ$ ) would remain very close to the reference value up to a constant. We furthermore compared (in Figure 6-(e)) the sum of CCC angle energies in these two parametrizations on a wide range of geometries of cyclopropane with three CCC angles  $\theta_0, \theta_1, \theta_2$  satisfying  $50^\circ < \theta_0 < 70^\circ, -10^\circ < \theta_1 - \theta_2 < 10^\circ$  and noticed that the difference is always a constant with fluctuations within 1 kcal/mol.

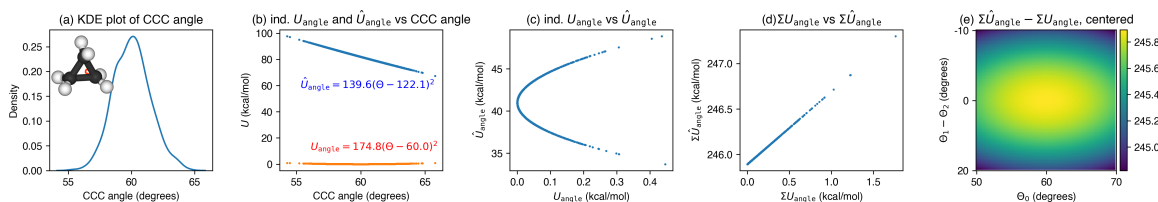


**Figure 6. A comparison of reference and Espaloma-learned parametrization of cyclopropane.** (a): KDE plot of CCC angle in cyclopropane. (b): **Individual** reference and predicted angle energy ( $U_{\text{angle}}$  and  $\hat{U}_{\text{angle}}$ , energy of each CCC angle) plotted against CCC angle values in the snapshots generated. (c): Predicted plotted against reference **individual** CCC energy. (d): Predicted plotted against reference **sum** CCC energy. (e): Distribution of difference between reference  $\Sigma U_{\text{angle}}$  and predicted  $\Sigma \hat{U}_{\text{angle}}$  **sum** CCC energy.

dataset	# mols	# trajs	# snapshots	Espaloma RMSE		Legacy FF RMSE (kcal/mol)			
				Train	Test	OpenFF 1.2.0	GAFF-1.81	GAFF-2.11	Amber ff14SB
<b>PhAlkEthOH</b> (simple CHO)	7408	12592	244036	0.8128 <sub>0.7603</sub> <sup>0.8521</sup>	1.0980 <sub>1.0375</sub> <sup>1.1629</sup>	1.6071 <sub>1.5197</sub> <sup>1.6915</sup>	1.7267 <sub>1.6543</sub> <sup>1.7935</sup>	1.7406 <sub>1.6679</sub> <sup>1.8148</sup>	
<b>OpenFF Gen2 Optimization</b> (druglike)	792	3977	23748	0.9452 <sub>0.8387</sub> <sup>1.0159</sup>	1.1342 <sub>1.0566</sub> <sup>1.2305</sup>	2.1768 <sub>2.0380</sub> <sup>2.3388</sup>	2.4274 <sub>2.3300</sub> <sup>2.5207</sup>	2.5386 <sub>2.4370</sub> <sup>2.6640</sup>	
<b>VEHICLE</b> (heterocyclic)	24867	24867	234326	0.9799 <sub>0.9350</sub> <sup>1.0371</sup>	0.9575 <sub>0.9121</sub> <sup>1.0365</sup>	8.0247 <sub>7.8215</sub> <sup>8.2456</sup>	8.0077 <sub>7.7647</sub> <sup>8.2313</sup>	9.4014 <sub>9.2135</sub> <sup>9.6434</sup>	
<b>PepConf</b> (peptides)	736	7560	22154	1.2511 <sub>1.1773</sub> <sup>1.3579</sup>	1.7041 <sub>1.6032</sub> <sup>1.8582</sup>	3.6143 <sub>3.4870</sub> <sup>3.7288</sup>	4.4446 <sub>4.3386</sub> <sup>4.5738</sup>	4.3356 <sub>4.1965</sub> <sup>4.4641</sup>	3.1502 <sub>3.1117</sub> <sup>3.1859*</sup>
<b>joint</b> OpenFF Gen2 Optimization	1528	11537	45902	0.7536 <sub>0.6974</sub> <sup>0.8297</sup>	1.8940 <sub>1.7913</sub> <sup>2.0194</sup>				
PepConf				1.1494 <sub>1.0907</sub> <sup>1.2274</sup>	1.6912 <sub>1.5748</sub> <sup>1.8524</sup>				

**Table 2. Espaloma can directly fit quantum chemical energies to produce a new molecular mechanics force fields with better accuracy than traditional force fields based on atom typing or direct chemical perception.** Espaloma was fit to quantum chemical potential energies for conformations generated by optimization trajectories from multiple conformers in various datasets from QCArchive [53]. All datasets were partitioned by molecules 80:10:10 into train:validate:test sets. We report the RMSE on training and test sets, as well as the performance of legacy force fields on the test set. All statistics are computed with predicted and reference energies centered to have zero mean for each molecule to focus on errors in relative conformational energetics, rather than on errors in predicting the heats of formation of chemical species (which the MM functional form used here is incapable of). The 95% confidence intervals annotated are calculated by via bootstrapping molecules with replacement using 1000 replicates. \*: Six cyclic peptides that cannot be parametrized using OpenForceField toolkit engine [87] and is not included.

## 5 Espaloma can fit quantum chemical energies directly to build new molecular mechanics force fields

Since Espaloma can derive a force field solely by fitting to energies (and optionally gradients), we repeat the end-to-end fitting experiment (Section 4) directly using a quantum chemical (QM) datasets used to build and evaluate MM force fields. We assessed the ability of Espaloma to learn several distinct quantum chemical datasets generated by the Open Force Field Initiative [88] and deposited in the MolSSI QCArchive [89]:

- **PhAlkEthOH**<sup>5</sup> is a collection of compounds containing only the elements carbon, hydrogen, and oxygen in compounds containing phenyl rings, alkanes, ketones, and alcohols [86]. Limited in elemental and chemical diversity, this dataset is chosen as a proof-of-concept to demonstrate the capability of Espaloma to fit and generalize quantum chemical energies when training data is sufficient to exhaustively cover the breadth of chemical environments.
- **OpenFF Gen2 Optimization**<sup>6</sup> consists of druglike molecules used in the parametrization of the Open Force Field 1.2.0 ("Parsley") small molecule force field [90]. This set was constructed by the Open Force Field Consortium from challenging molecule structures provided by Pfizer, Bayer, and Roche, along with diverse molecules selected from eMolecules to achieve useful coverage of chemical space.

<sup>5</sup><https://github.com/openforcefield/qca-dataset-submission/tree/master/submissions/2020-09-18-OpenFF-Sandbox-CHO-PhAlkEthOH>

<sup>6</sup><https://github.com/openforcefield/qca-dataset-submission/tree/master/submissions/2020-03-12-OpenFF-Gen-2-Torsion-Set-1-Roche>, <https://github.com/openforcefield/qca-dataset-submission/tree/master/submissions/2020-03-12-OpenFF-Gen-2-Torsion-Set-2-Coverage>, <https://github.com/openforcefield/qca-dataset-submission/tree/master/submissions/2020-03-12-OpenFF-Gen-2-Torsion-Set-3-Pfizer-Discrepancy>, <https://github.com/openforcefield/qca-dataset-submission/tree/master/submissions/2020-03-12-OpenFF-Gen-2-Torsion-Set-4-eMolecules-Discrepancy>, <https://github.com/openforcefield/qca-dataset-submission/tree/master/submissions/2020-03-12-OpenFF-Gen-2-Torsion-Set-5-Bayer>

- **VEHICLE**<sup>7</sup> or *virtual exploratory heterocyclic library*, is a set of heteroaromatic ring systems of interest to drug discovery enumerated by Pitt et al. [91]. The atoms in the molecules in this dataset have interesting chemical environments in heteroaromatic rings that present a challenge to traditional atom typing schemes, which cannot easily accommodate the nuanced distinctions in chemical environments that lead to perturbations in heterocycle structure. We use this dataset to illustrate that Espaloma performs in situations challenging to traditional force fields.
- **PepConf**<sup>8</sup> from Prasad et al. [92] contains a variety of short peptides, including capped, cyclic, and disulfide-bonded peptides. This dataset—regenerated using the Open Force Field QCSUBMIT tool—explores the applicability of Espaloma to biopolymers, such as proteins.

Since nonbonded terms are generally optimized to fit other condensed-phase properties, we focused here on optimizing only the valence parameters (bond, angle, and proper and improper torsion) to fit these gas-phase quantum chemical datasets, fixing the non-bonded energies using a legacy force field [88]. All the non-bonded energies (Lennard-Jones and electrostatics) were computed using Open Force Field 1.2 Parsley [93], with AM1-BCC charges generated by the OpenEye Toolkit back-end for the Open Force Field toolkit 0.10.0 [87]. Because we are learning an MM force field that is incapable of reproducing quantum chemical heats of formation reflected as an additive offset in the quantum chemical energy targets, in both training and test sets, snapshot energies for each molecule are shifted to have zero mean. All datasets are randomly shuffled and split (by molecules) into training (80%), validation (10%), and test (10%) sets.

To assess how well Espaloma is able to generalize to new molecules, the performance for Espaloma on test (and training) sets was compared to a legacy atom typing based force field (GAFF 1.81 and 2.11 [52, 53]) and a modern force field based on direct chemical perception [21] (the Open Force Field 1.2.0 ("Parsley") small molecule force field [59]). The results of this experiment are reported in Table 2. As can be readily seen by the reported test set root mean squared error (RMSE), Espaloma can produce MM force fields with generalization performance consistently on par with, or better than, legacy force fields based on discrete atom typing (GAFF [52, 53]). Surprisingly, even though OpenFF 1.2.0 included the "Parsley" dataset in training, Espaloma is able to achieve superior *test* set performance on this dataset, suggesting both the flexibility and generalizability of continuous atom typing has significant advantages over even direct chemical perception [21].

We next examined whether the resulting Espaloma force field not only quantitatively reproduced quantum chemical equilibrium conformational energetics, but was able to also qualitatively preserve quantum chemical local minima. To assess this, we initiated MM energy minimizations from QM-optimized conformations from the test set of OpenFF Gen 2 Optimization dataset. Specifically, we selected the minimum quantum chemical energy snapshot for each molecule in the Parsley dataset and minimized with Espaloma-derived force field, OpenFF 1.2.0, GAFF 1.81, or GAFF 2.11 MM force fields using an L-BFGS optimizer with a 0.1 kJ/mol convergence tolerance. Figure 7 shows a kernel density estimate (KDE) of the root mean squared distance (RMSD) from the quantum chemical minimum produced by each force field. The Espaloma force field constructed from the OpenFF Gen 2 Optimization dataset achieved lower average RMSD when compared to GAFF 1.81 and GAFF 2.11, although a slightly higher average RMSD was obtained than OpenFF 1.2.0. Again, note that OpenFF 1.2.0 is trained on this dataset. Qualitatively, although the peak of the KDE for Espaloma-parametrized force fields appears at a higher-RMSD region than those of the representative legacy force fields, the high-RMSD tail of the KDE (which represents large conformational discrepancies) for Espaloma is highly depleted compared to the other force fields, suggesting the frequency of severe errors is greatly reduced.

## 6 Espaloma can integrate fully differentiable self-consistent charge models

Historically, biopolymer force fields derive partial atomic charges via fits to high-level multiconformer quantum chemical electrostatic potentials on capped model compounds adjusted to ensure the repeating biopolymer units have integral charge (often incorporating constraints to share identical backbone partial charges) [48,

<sup>7</sup><https://github.com/openforcefield/qca-dataset-submission/tree/master/submissions/2019-07-02%20VEHICLE%20optimization%20dataset>

<sup>8</sup><https://github.com/openforcefield/qca-dataset-submission/tree/master/submissions/2020-10-26-PEPCONF-Optimization>

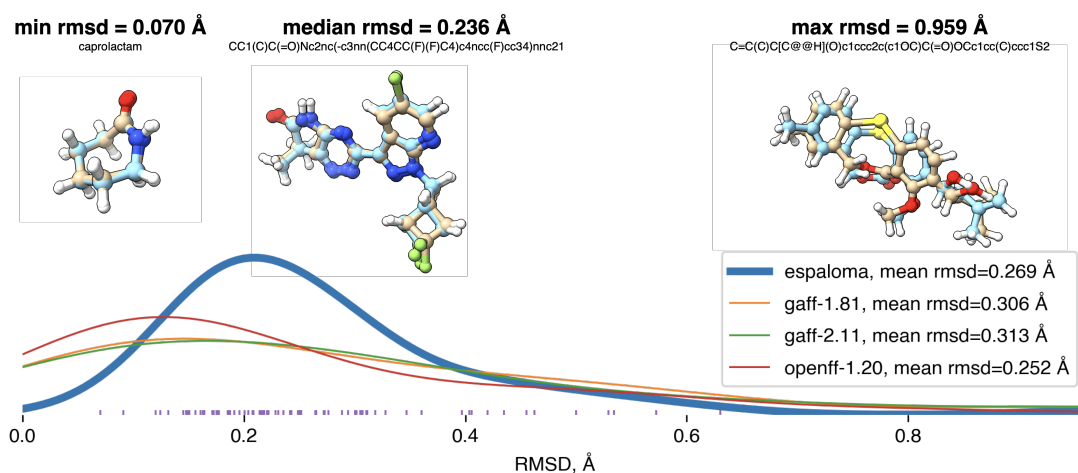


**Figure 7. Espaloma-derived molecular mechanics force fields preserve the location of quantum chemical minima.** Kernel density estimate (KDE) plot of root mean square deviation (RMSD) between quantum chemical minima and MM-optimized minima using parameters from either **Espaloma**-generated molecular mechanics or legacy force fields. The overlaid structures depict quantum chemical minima (in cyan) and Espaloma minima (in gold) of typical structures with minimum, median, and maximum RMSD.

94, 95]. Some approaches to the derivation of partial atomic charges are enormously expensive, requiring iterative QM/MM simulations in explicit solvent to derive partial charges for new molecules [96, 97]. For small molecules, state-of-the-art methods range from fast bond charge corrections applied to charges derived from semiempirical quantum chemical methods (such as AM1-BCC [98, 99] or CGenFF charge increments [80]) to expensive multiconformer restrained electrostatic potential (RESP) fits to high-level quantum chemistry [100, 101]. Surprisingly little attention has been paid to the divergence of methods used for assigning partial charges to small molecules and biopolymers and the potential impact this inconsistency has on accuracy or ease of use—indeed, developing charges for post-translational modifications to biopolymer residues [102] or covalent ligands can prove to be a significant technical challenge in attempting to bridge these two worlds.

While machine learning approaches have begun to find application in determining small molecule partial charges [103–105], methods such as random forests are not fully continuously differentiable, rendering them unsuitable for a fully end-to-end differentiable parameter assignment framework. Recently, we proposed a fast approach that uses graph neural networks as part of a charge-equilibration [106] scheme (inspired by the earlier VCharge model [107]) to self-consistently assign partial charges to small molecules, biopolymers, and arbitrarily complex hybrid molecules in a conformation-independent manner that only makes use of molecular topology [29]. Perhaps unsurprisingly, due to the requirement that molecules retain their integral net charge, directly predicting partial atomic charges from latent atom embeddings and subsequently renormalizing charges leads to poor performance [29].

Instead, predicting the parameters of a simple physical topological charge-equilibration model [106, 107] can provide very high accuracy in reproducing partial charges derived from high-level quantum chemical electrostatic potential fits [29]. Specifically, we use our atom latent representation to instead predict the first- and second-order derivatives of a pseudopotential energy  $E$  with respect to the partial atomic charge  $q_i$  on atom  $i$ :

$$e_i \equiv \frac{\partial E}{\partial q_i}, s_i \equiv \frac{\partial^2 E}{\partial^2 q_i}. \quad (32)$$

Here, the *electronegativity*  $e_i$  quantifies the desire for an atom to take up negative charge, while the *hardness*  $s_i$  quantifies the resistance to gaining or losing too much charge. A module is added to Stage III of Espaloma to predict the chemical environment adapted  $(e_i, s_i)$  parameters for each atom from the latent atom embeddings.

The partial charges for all atoms can then be obtained by minimizing the second-order Taylor expansion of the potential pseudoenergy contributed by atomic charges:

$$\{\hat{q}_i\} = \operatorname{argmin}_{q_i} \sum_i \hat{e}_i q_i + \frac{1}{2} \hat{s}_i q_i^2, \quad (33)$$

subject to

$$\sum_i \hat{q}_i = \sum_i q_i = Q, \quad (34)$$

where  $Q$  is the total (net) charge of the molecule.

Using Lagrange multipliers, the solution to 33 can be given analytically by:

$$\hat{q}_i = -e_i s_i^{-1} + s_i^{-1} \frac{Q + \sum_i e_i s_i^{-1}}{\sum_j s_j^{-1}}, \quad (35)$$

whose Jacobian and Hessian are trivially easy to calculate. As a result, the prediction of  $\{\hat{e}_i, \hat{s}_i\}$  could be optimized end-to-end using backpropagation.

We integrated this approach into an Espaloma model where parameters of the charge equilibrium model  $\{e_i, s_i\}$  and the bonded (bond, angle, and torsion) parameters are optimized jointly. The resulting model is trained by augmenting the loss function to include a term that penalizes the deviation from AM1-BCC partial charges for the molecules in the training set. As shown in Table 3, even without fine-tuning the weights of these two terms (the loss functions are simply summed up), the joint model achieves better performance compared to independent models trained on either tasks.

	charge RMSE (e)		energy RMSE (kcal/mol)	
	training	test	training	test
charge model only	0.0137 <sup>0.0144</sup> <sub>0.0131</sub>	0.0308 <sup>0.0369</sup> <sub>0.0269</sub>		
energy model only*			0.9452 <sup>1.0159</sup> <sub>0.8887</sub>	1.1342 <sup>1.2305</sup> <sub>1.0566</sub>
joint valence energy + charge model	0.0134 <sup>0.0140</sup> <sub>0.0127</sub>	0.0291 <sup>0.0332</sup> <sub>0.0253</sub>	0.8240 <sup>0.8911</sup> <sub>0.7724</sub>	0.9241 <sup>1.0183</sup> <sub>0.8303</sub>

**Table 3. Espaloma can jointly predict partial charges through a simple charge-equilibration model that learns electronegativity and hardness parameters.** Using OpenFF Gen 2 Optimization dataset (which Open Force Field 1.2.0 [59] is trained on), in the first two rows, we train two independent models to predict the energy of conformations and charges of atoms; in the third row, we use a joint model where the latent embedding is shared between these two tasks. We observe that joint model outperforms the independent model in both tasks. As a reference, the RMSE between AM1-BCC charges assigned by two different cheminformatics toolkits—Ambertools 21 [52] and OpenEye Toolkit—are 0.0237<sup>0.0251</sup><sub>0.0221</sub> (e). \*: Same experiment as Table 2.

## 7 Espaloma can parameterize biopolymers

The speed and flexibility of graph convolutional networks allows Espaloma to parameterize even very large biopolymers, treating them as (large) small molecules in a graph-theoretical manner. While graph nets perceive nonlocal aspects of the chemical environment around each atom, the limited number of rounds of message passing ensures stability of the resulting parameters when parameterizing systems that consist of repeating residues, like proteins and nucleic acids.

To demonstrate this, we considered the simple polypeptide system ACE-ALA<sub>n</sub>-NME, consisting of  $n$  alanine residues terminally capped by acetyl- and N-methyl amide capping groups. Using the joint charge and valence term Espaloma model, we assigned parameters to ACE-ALA<sub>n</sub>-NME systems with  $n = 1, 2, \dots, 500$ , showing illustrative parameters in Figure 8. Espaloma stably assigns parameters to the interior residues of peptides even as they increase in length, with parameters of the central residue unchanged after  $n > 3$ . This pleasantly resembles the behavior of traditional residue template based protein force fields, even though no templates are used within Espaloma’s parameter assignment process.

Despite its use of a sophisticated graph net machine learning model, the wall time required to parameterize large protein scales linearly with respect to the number of residues (and hence system size) on a CPU

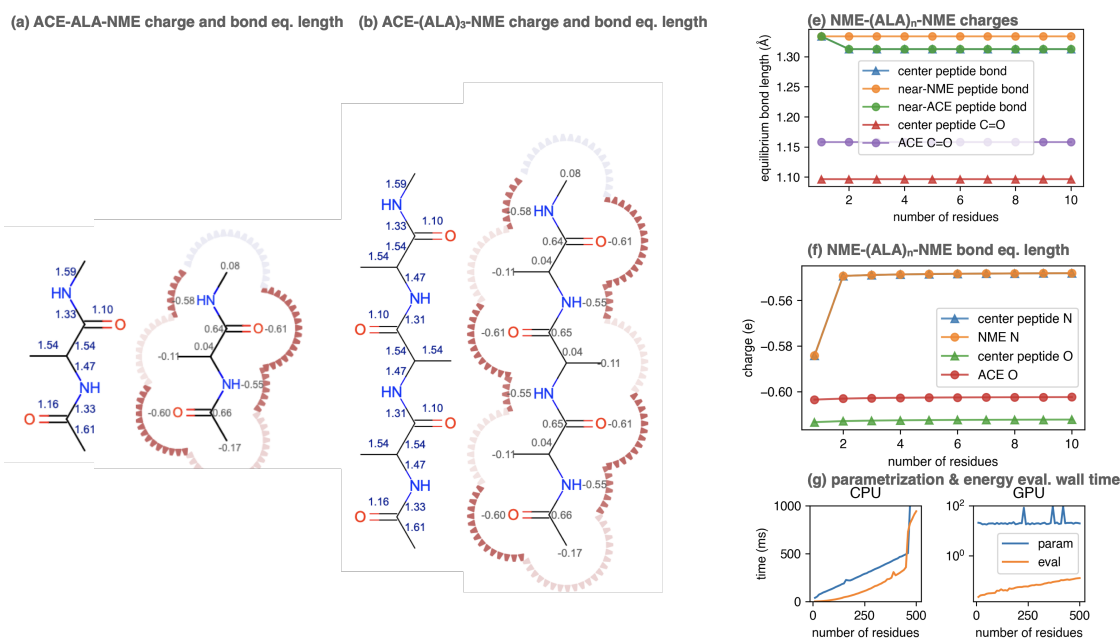


**Figure 8. Espaloma can be used to generate self-consistent force fields for biopolymers and small molecules.** (a) Espaloma-assigned equilibrium heavy atom bond lengths (left, in angstrom) and heavy atom partial charges (right, in elemental charge unit) for ACE-(ALA)<sub>1</sub>-NME. (b) Espaloma-assigned equilibrium heavy atom bond lengths (left) and heavy atom partial charges (right) for ACE-(ALA)<sub>3</sub>-NME, which shows minimal deviation from ACE-(ALA)<sub>1</sub>-NME and consistent parameters for amino acid residues. (c) Partial atomic charges of selected atoms shown for ACE-(ALA)<sub>n</sub>-NME for  $n = 1, \dots, 10$ . (d) Equilibrium bond lengths of selected bonds for ACE-(ALA)<sub>n</sub>-NME for  $n = 1, \dots, 10$ . (e) CPU (left) and GPU (right) parameter assignment (blue curve) and energy evaluation on OpenMM 7.5.1 [108] (orange curve) wall times.

(Figure 8, lower right). On a GPU, the wall clock time needed to parameterize systems up to this size stays roughly constant (due to overhead in executing models on the GPU) at less than 100 microseconds. Since Espaloma applies standard molecular mechanics force fields, the energy evaluation time for an Espaloma-generated force field are identical to traditional force fields.

## 8 Espaloma can produce self-consistent biopolymer and small molecule force fields that result in stable simulations

Traditionally, in a protein-ligand system, separate (but hopefully compatible) force fields and charge models have been assigned to small molecules (which are treated as independent entities parameterized holistically) and proteins (which are treated as collections of templated residues parameterized piecemeal) [109]. This practice both has the potential to allow significant inconsistencies while also introducing significant complexity in parameterizing heterogeneous systems.

Using the joint Espaloma model trained on both the "OpenFF Gen 2 Optimization" small molecule and "PepConf" peptide quantum chemical datasets (Section 5) [110, 111]), we can apply a consistent set of parameters to both protein and small molecule components of a kinase:inhibitor system. Figure ?? shows the ligand heavy-atom RMSD after aligning on protein heavy atoms for 0.5 ns trajectories Tyk2:inhibitor system from the Alchemical Best Practices Benchmark Set 1.0 [112]. It is readily apparent that the Espaloma-derived parameters lead to trajectories that are comparably stable to simulations that utilize the Amber ff14SB protein force field [47] with GAFF 1.81, GAFF 2.11 [52, 53], or OpenFF 1.2.0 [59] small molecule force fields. All systems are explicitly solvated with a 9 Å buffer around the protein with TIP3P water [113] and use the Joung and Cheatham monovalent counterion parameters [114] to model a neutral system with 300 mM NaCl salt.

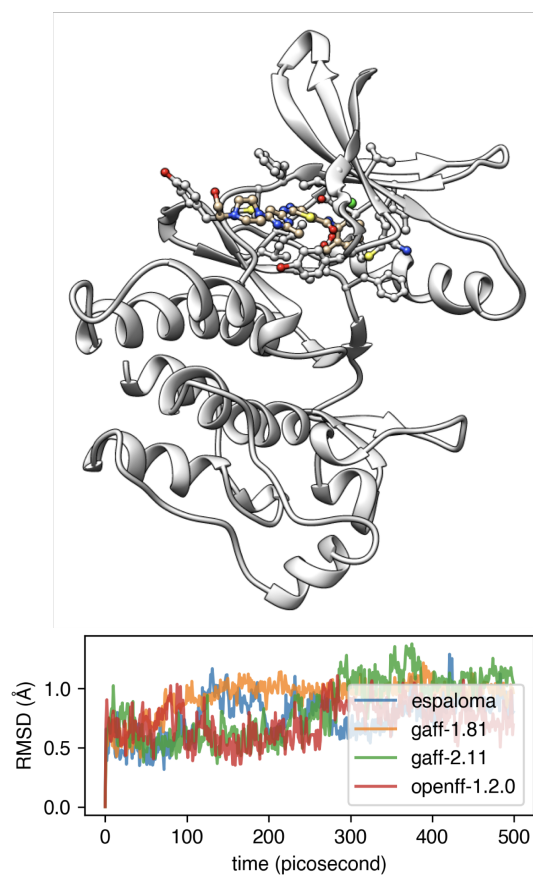


**Figure 9. Espaloma simultaneously parametrizes marco- and small molecule in protein-ligand system.** Top: Tyrosine kinase 2 system parametrized by Espaloma and minimized and equilibrated with TIP3P water model [69] and counterions. Bottom: Root mean-squared displacement (RMSD) of ligand w.r.t. the initial position, in systems parametrized by Espaloma and traditional force fields.

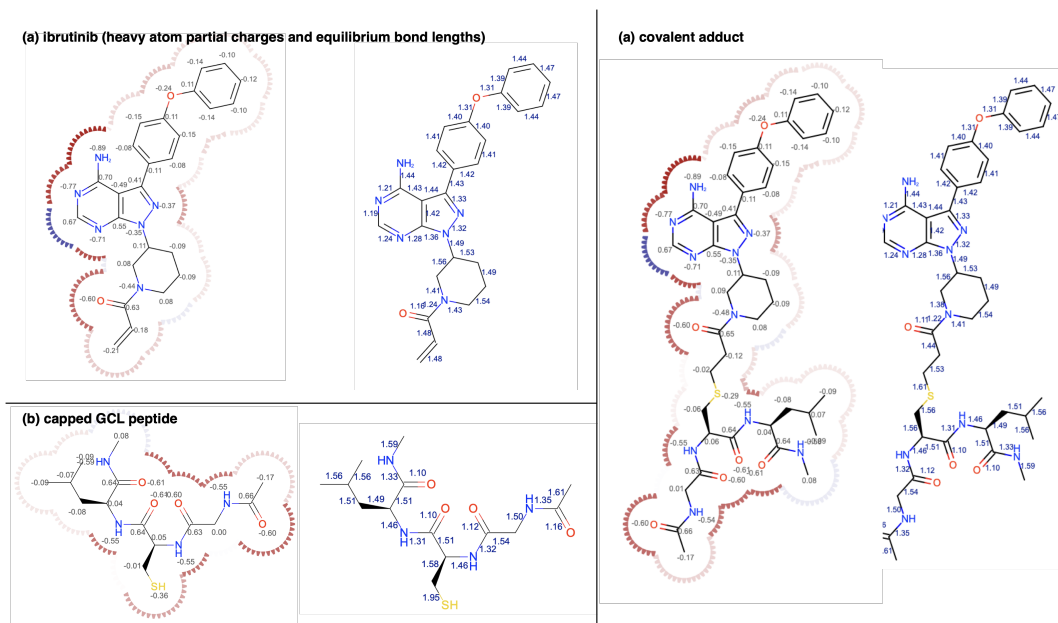


**Figure 10. Espaloma parametrizes covalent inhibitor adduct system.** Heavy atom bond equilibrium length (in angstrom) and partial charge (in elemental charge) prediction for (a) ibrutinib; (b) capped GCL peptide; and (c) their covalent adduct.

## 9 Espaloma can easily parameterize complex heterogeneous biomolecular systems

While biomolecular systems of interest are often highly heterogeneous environments, it is often practically incredibly difficult to model systems that consist of more than the simplest protein-ligand-solvent combinations. For example, the latest Amber 20 release [109] recommends a set of independently developed (but loosely coupled) set of force fields and complex parameterization machinery for proteins [47], DNA [115], RNA [116], water [113], monovalent [114, 117] and divalent [118–120] counterions, lipids [121], carbohydrates [122], glycoconjugates [123, 124], small molecules [52, 53], post-translational modifications [102], nucleic acid modifications [125], collectively representing hundreds of human-years of effort. Despite this, even seemingly simple common tasks—such as modeling irreversible covalent inhibitors—represent a mind-bending technical challenge for parameterization [126].

Espaloma operates on only the chemical graph of components of the system, which enables it to solve many issues with these legacy approaches: In generating parameters, there is no practical difference between any of the biopolymer, biomolecule, organic molecule, solvent, ion, or covalently modified species that previously required enormous effort to separately build parameter sets to cover; Espaloma will simply interpolate the parameters from observed examples in a continuous manner. Instead of separately curating distinct datasets and philosophies for parameterizing each of these different classes of chemical species, extending an Espaloma model to a new class of chemical species is simply a matter of extending the training datasets of quantum chemical and/or physical property data. As we have seen, building an elementary model capable of simulating solvated protein-ligand complexes simply required incorporating quantum chemical datasets used to parameterize a small molecule force field alongside quantum chemical data for short peptides.

This Espaloma model should also provide sufficient coverage to model more complex protein-ligand covalent conjugates, since the relevant chemistry to model this complex already exists in the training dataset. To demonstrate this leads to stable, sensible parameters, we considered the pre-reactive form of the covalent kinase inhibitor ibrutinib and the terminally-blocked form of the Val-Cys-Gly sequence that it reacts with in its target kinase BTK (Figure 10, left). Espaloma is able to rapidly parameterize the covalent conjugate of ibrutinib to this BTK target sequence, resulting in minor changes to parameters and partial charges around

the covalent warhead, but minimally perturbing the remainder of the system (Figure 10, right). Unlike legacy approaches to parameterizing covalently-modified residues, no expensive parameter or charge refinement procedure was needed for this task.

## 10 Discussion

Here, we have demonstrated that graph neural networks not only have the capacity to reproduce legacy atom type classification, but they are sufficiently expressive to fit a traditional molecular mechanics force field, generalize it to new molecules, as well as learn entirely new force fields directly from quantum chemical energies and experimental measurements. The neural framework presented here also affords the modularity to easily experiment with the inclusion of additional potential energy terms, functional forms, or parameter classes, while making it easy to rapidly refit the entire force field afterwards.

### Espaloma enables a wide variety of applications

Espaloma enables a wide variety of applications in the realm of molecular simulation: While many force field packages use complex, difficult to maintain, non-portable custom typing engines [53–55, 127], simply generating examples is sufficient to train Espaloma to reproduce this typing, translating it into a model that is easy to extend by providing more quantum chemical training data. Some force fields have traditionally been typed by hand, making them difficult to automate [127]; Espaloma can in principle learn to generalize from these examples, provided care is taken to avoid overfitting during training. As we have shown here, Espaloma also provides a convenient way to rapidly build new force fields directly from quantum chemical data.

### Espaloma enables simultaneous fitting to quantum chemical and experimental condensed phase physical properties and free energy measurements

In typical approaches to force field parameterization, nonbonded parameters—such as Lennard-Jones potentials to model van der Waals interactions and partial charges to model electrostatic interactions—are fit to reproduce physical properties (such as densities and enthalpies of vaporization) for simple liquids or liquids mixtures [68, 69, 74, 76, 77, 113, 128]. While here we have primarily focused on learning valence parameters from quantum chemistry (Section 5), physical properties—such as free energies of hydration—can be used in an objective function where automatic differentiation can appropriately propagate the gradients back to allow automatic optimization of the entire typing and parameter assignment process. While this approach could easily be extended to fit the standard assortment of physical properties simultaneously with fitting quantum chemical data, it tantalizingly offers the opportunity to go further by incorporating experimental data derived from transfer free energies, such as binding free energies of small molecules to macromolecular hosts [129, 130] or proteins, partition or distribution coefficients [131, 132], or relative solubilities [133, 134] and activity coefficients [135]. Our demonstration on fitting hydration free energies for an implicit solvent model is in principle no different from the approach that would be used for explicit solvent or condensed-phase properties, except that some form of bridging simulations are required to provide adequate overlap, from which parameter gradients to be efficiently computed with multistate reweighting techniques like MBAR [136]. This approach has recently been used to refit a quantum machine learning force field to experimental free energies [137].

Fitting to both condensed-phase data and quantum chemical data will inevitably require some form of weighting between different components of the objective or loss function to balance the contributions to the parameter gradient during optimization; methods like ForceBalance have arrived at convenient approaches for balancing quantum chemical and experimental data classes [23]. If the goal is to reproduce physical properties of interest, one could consider the quantum chemical data as more of a "regularizer" in aiding the model in exploring robust regions of physical model space, perhaps augmented by additional terms in the loss function that ensure parameters end up in physical regions of parameter space. If a fully Bayesian approach is adopted, these could even be enforced as some form of model prior.

## Modern machine learning frameworks offer flexibility in fitting potentials

The flexibility afforded by modern machine learning frameworks solves a long-standing problem in molecular simulation in which it is extremely difficult to assess whether a new functional form might lead to significant benefits in modeling multiple properties of interest. While efforts such as the Open Force Field Initiative aim to streamline the process of refitting force fields [110], the ease of refitting models in machine learning frameworks makes it extremely easy to experiment with new functional forms: Modern automatic differentiation in these frameworks means that only the potential need be implemented, and gradients are automatically computed.

This enables a wide variety of exploration: Simple improvements could be widely implemented in current molecular simulation packages include adjusting the 1-4 Lennard-Jones and electrostatics scaling parameters, producing 1-4 interaction parameters that override Lennard-Jones combining rules, exploring different Lennard-Jones combining rules [50], changing the van der Waals treatment to alternative functional forms (such as Buckingham exp-6 [138] or Halgren potentials [60]), and refitting force fields for various non-bonded treatments (such as PME [139] and reaction field electrostatics [140]). Many simulation packages provide support for Class II molecular mechanics force fields [40, 41], which include additional coupling terms that can drastically reduce errors in modeling quantum chemical energies at essentially no meaningful impact on cost due to the  $\mathcal{O}(N)$  number of these terms; simple extensions to Espaloma's architecture can easily predict the parameters for these coupling from additional symmetry-preserving features.

More radical potential explorations could involve assessing different algebraic functional forms—modern simulation packages such as OpenMM have the ability to automatically differentiate and compile symbolic algebraic expressions to produce optimized force kernels for simulation on fast GPUs [16, 108]. Excitingly, the simplicity of incorporating a new generation of quantum machine learning (QML) potentials [141]—such as ANI [10, 13] and SchNet [14]—means that it will be easy to explore hybrid potentials that combine the flexibility of QML potentials at short range with the accuracy of physical forces at long range [142].

## Espaloma can enable fully Bayesian force field parameterization and model uncertainty quantification

While much of the history of molecular simulation has focused on quantifying the impact of statistical uncertainty [143–145], critical studies over the last decade [146–155] have improved our ability to quantify and propagate predictive uncertainty in molecular mechanics force fields by quantifying contributions from model uncertainty—which is frequently the major source of predictive uncertainty in applications of interest. While most attention has been focused on the *continuous parameters* of the force field model with fixed model form, some progress has been made in discrete model selection among candidate model forms [156–158].

It remains an open problem to rigorously quantify uncertainty in other important parts of the model definition—especially in the definitions of atom-types. These “chemical perception” definitions can involve very large spaces of discrete choices, and crucially influence the behavior of a generalizable molecular mechanics model [21, 159].

An important benefit of the present approach is that it reduces the mixed continuous-discrete task of “being Bayesian about atom-types” to the more familiar task of “being Bayesian about neural network weights.” Bayesian treatment of neural networks—while also intractable—has been the focus of productive study and methodological innovation for decades [160].

We anticipate that Bayesian extensions of this work will enable more comprehensive treatment of predictive uncertainty in molecular mechanics force fields.

## Challenges remain in robust optimization of Espaloma models

While recasting the force field construction problem as an end-to-end differentiable machine learning problem affords numerous advantages, several familiar challenges remain. We note that training error did not go to zero in the MM model recovery task (section 4), as we had initially expected. This could be reflective of limited model expressiveness, difficulty of numerical optimization, or an implementation error. The evidence so far reduces suspicion of limited model expressiveness, and the fact that this behavior persists even

when considering restricted functional forms suggests that the issue is not solely due to implementation. Defining parameter initialization and optimization procedures that perform more robustly for differentiable models that contain valence force fields in the loop is an important avenue for follow-up work.

Ensuring full chemical equivalence is nontrivial

In the current experiments, Espaloma used a set of atom features (one-hot encoded element, hybridization, aromaticity, formal charge, and membership in rings of various sizes) easily computed using a cheminformatics toolkit; no bond features were used (see **Detailed Methods**). While this provided excellent performance, the non-uniqueness of formal charge assignment (obvious in molecules such as guanidinium where resonance forms locate the formal charge on different atoms) does not guarantee the assigned parameters will respect chemical equivalence (a form of invariance) in cases where these atom properties are not unique. Ensuring full chemical equivalence would require modifications to this strategy, such as omission of non-unique features (which may require additional data or pre-training to learn equivalent chemical information), averaging of the output of one or more stages over equivalent resonance forms, or architectures such as transformers that more fully encode chemical equivalence.

## 11 Detailed Methods

### 11.1 Code Availability

The Python code used to produce the results discussed in this paper is distributed open source under MIT license [<https://github.com/choderalab/espaloma>]. Core dependencies include PyTorch 1.9.1 [161], Deep Graph Library 0.6.0 [34], the Open Force Field Toolkit 0.10.0 [88, 162], and OpenMM 7.5.1 [16].

### 11.2 Datasets

The typed ZINC validation subset distributed with parmFrosst [83] was used in atom typing classification experiments (Section 3).

For MM fitting experiments (Section 4), we employed molecules the PhAlkEthOH dataset [86], parametrized with GAFF-1.81 [84] using Antechamber [52, 53] from AmberTools21, and generated molecular dynamics (MD) snapshots with annotated energies according to the procedure detailed below (Section 11.4). We filter out molecules with a gap between minimum and maximum energy larger than 0.1 Hartree (62.5 kcal/mol).

For QM fitting experiments (Section 5), datasets hosted on QCArchive [89] are used. We filter out snapshots with energies higher than 0.1 Hartree (62.5 kcal/mol) higher than the minima. Within all datasets, we randomly select training, test, and validation sets with 80:10:10 partitions.

### 11.3 Machine learning experimental details

The input features of the atoms included the one-hot encoded element, as well as the hybridization, aromaticity, (various sized-) ring membership, and formal charge thereof, assigned using the Open Force Field toolkit 0.10.0 [162] using the OpenEye backend.

All models are trained with 5000 epochs with the Adam optimizer [163]; early stopping was used to select the epoch with lowest validation set loss.

Hyperparameters, namely choices of graph neural network layer architectures (GIN [28], GCN [30], GraphSAGE [164], SGConv [165]), depth of graph neural network and of Janossy pooling network (3, 4, 5, 6), activation functions (ReLU, sigmoid, tanh), learning rates (1e-3, 1e-4, 1e-5), and per-layer units (16, 32, 64, 128, 256, 512) were briefly optimized with a grid search using validation sets on the MM fitting experiment. As a result, we use three 128-units GraphSAGE [164] layers with ReLU activation function for stage I and four 128-units feed-forward layers with ReLU activation for stage II and III. Reported metrics:  $R^2$ : the coefficient of determination, RMSE: root mean square error, MAPE: mean absolute percentage error; note that the MAPE results we report is not multiplied by 100, and therefore denotes the fractional error. The annotated 95% confidence intervals are calculated by bootstrapping the test set 1000 times to account for finite-size effects in the composition of the test set.

## 11.4 Molecular dynamics simulation details

High-temperature MD simulations described in Section 4 were initialized using RDKit's default conformer generator followed by energy minimization in OpenMM 7.5, with initial velocities assigned randomly to the target temperature. Vacuum trajectories were simulated without constraints using `LangevinIntegrator` from OpenMM [16] using a temperature of 500 K, collision rate of 1/picosecond, and a timestep of 1 fs. 500 samples (5 ns) are collected with 10000 steps (10 ps) between each sample.

## References

- [1] Jay W Ponder and David A Case. Force fields for protein simulations. In *Advances in protein chemistry*, volume 66, pages 27–85. Elsevier, 2003.
- [2] David Van Der Spoel, Erik Lindahl, Berk Hess, Gerrit Groenhof, Alan E Mark, and Herman JC Berendsen. Gromacs: fast, flexible, and free. *Journal of computational chemistry*, 26(16):1701–1718, 2005.
- [3] David A Case, Thomas E Cheatham III, Tom Darden, Holger Gohlke, Ray Luo, Kenneth M Merz Jr, Alexey Onufriev, Carlos Simmerling, Bing Wang, and Robert J Woods. The amber biomolecular simulation programs. *Journal of computational chemistry*, 26(16):1668–1688, 2005.
- [4] James C Phillips, Rosemary Braun, Wei Wang, James Gumbart, Emad Tajkhorshid, Elizabeth Villa, Christophe Chipot, Robert D Skeel, Laxmikant Kale, and Klaus Schulten. Scalable molecular dynamics with namd. *Journal of computational chemistry*, 26(16):1781–1802, 2005.
- [5] Free Energy Calculations. Theory and applications in chemistry and biology. *Springer Series in Chemical Physics*, 86, 2007.
- [6] C.C. Wang, G. Pilania, S.A. Boggs, S. Kumar, C. Breneman, and R. Ramprasad. Computational strategies for polymer dielectrics design. *Polymer*, 55(4):979 – 988, 2014. ISSN 0032-3861. doi: <https://doi.org/10.1016/j.polymer.2013.12.069>. URL <http://www.sciencedirect.com/science/article/pii/S0032386113011889>.
- [7] Chunyu Li and Alejandro Strachan. Molecular scale simulations on thermoset polymers: A review. *Journal of Polymer Science Part B: Polymer Physics*, 53(2):103–122, 2015.
- [8] Huai Sun, Zhao Jin, Chunwei Yang, Reinier LC Akkermans, Struan H Robertson, Neil A Spenley, Simon Miller, and Stephen M Todd. Compass ii: extended coverage for polymer and drug-like molecule databases. *Journal of molecular modeling*, 22(2):47, 2016.
- [9] Edward Harder, Wolfgang Damm, Jon Maple, Chuanjie Wu, Mark Reboul, Jin Yu Xiang, Lingle Wang, Dmitry Lupyan, Markus K Dahlgren, Jennifer L Knight, et al. Opls3: a force field providing broad coverage of drug-like small molecules and proteins. *Journal of chemical theory and computation*, 12(1):281–296, 2016.
- [10] Justin S Smith, Olexandr Isayev, and Adrian E Roitberg. Ani-1: an extensible neural network potential with dft accuracy at force field computational cost. *Chemical science*, 8(4):3192–3203, 2017.
- [11] Justin S Smith, Ben Nebgen, Nicholas Lubbers, Olexandr Isayev, and Adrian E Roitberg. Less is more: Sampling chemical space with active learning. *The Journal of chemical physics*, 148(24):241733, 2018.
- [12] Justin S Smith, Benjamin T Nebgen, Roman Zubatyuk, Nicholas Lubbers, Christian Devereux, Kipton Barros, Sergei Tretiak, Olexandr Isayev, and Adrian E Roitberg. Approaching coupled cluster accuracy with a general-purpose neural network potential through transfer learning. *Nature communications*, 10(1):1–8, 2019.
- [13] Christian Devereux, Justin S Smith, Kate K Davis, Kipton Barros, Roman Zubatyuk, Olexandr Isayev, and Adrian E Roitberg. Extending the applicability of the ani deep learning molecular potential to sulfur and halogens. *Journal of Chemical Theory and Computation*, 16(7):4192–4202, 2020.
- [14] Kristof T Schütt, Huziel E Sauceda, P-J Kindermans, Alexandre Tkatchenko, and K-R Müller. Schnet—a deep learning architecture for molecules and materials. *The Journal of Chemical Physics*, 148(24):241722, 2018.
- [15] Simon Batzner, Tess E Smidt, Lixin Sun, Jonathan P Mailoa, Mordechai Kornbluth, Nicola Molinari, and Boris Kozinsky. Se (3)-equivariant graph neural networks for data-efficient and accurate interatomic potentials. *arXiv preprint arXiv:2101.03164*, 2021.
- [16] Peter Eastman, Jason Swails, John D Chodera, Robert T McGibbon, Yutong Zhao, Kyle A Beauchamp, Lee-Ping Wang, Andrew C Simmonett, Matthew P Harrigan, Chaya D Stern, et al. Openmm 7: Rapid development of high performance algorithms for molecular dynamics. *PLoS computational biology*, 13(7):e1005659, 2017.

- [17] Matt J Harvey, Giovanni Giupponi, and G De Fabritiis. Acemd: accelerating biomolecular dynamics in the microsecond time scale. *Journal of chemical theory and computation*, 5(6):1632–1639, 2009.
- [18] Romelia Salomon-Ferrer, Andreas W Gotz, Duncan Poole, Scott Le Grand, and Ross C Walker. Routine microsecond molecular dynamics simulations with amber on gpus. 2. explicit solvent particle mesh ewald. *Journal of chemical theory and computation*, 9(9):3878–3888, 2013.
- [19] Samuel S. Schoenholz and Ekin D. Cubuk. Jax, m.d.: End-to-end differentiable, hardware accelerated, molecular dynamics in pure python, 2019.
- [20] Wujie Wang, Simon Axelrod, and Rafael Gómez-Bombarelli. Differentiable molecular simulations for control and learning, 2020.
- [21] David L Mobley, Caitlin C Bannan, Andrea Rizzi, Christopher I Bayly, John D Chodera, Victoria T Lim, Nathan M Lim, Kyle A Beauchamp, David R Slochow, Michael R Shirts, et al. Escaping atom types in force fields using direct chemical perception. *Journal of chemical theory and computation*, 14(11):6076–6092, 2018.
- [22] Lee-Ping Wang, Jiahao Chen, and Troy Van Voorhis. Systematic parametrization of polarizable force fields from quantum chemistry data. *Journal of Chemical Theory and Computation*, 9(1):452–460, November 2012. doi: 10.1021/ct300826t. URL <https://doi.org/10.1021/ct300826t>.
- [23] Lee-Ping Wang, Todd J. Martinez, and Vijay S. Pande. Building force fields: An automatic, systematic, and reproducible approach. *The Journal of Physical Chemistry Letters*, 5(11):1885–1891, May 2014. doi: 10.1021/jz500737m. URL <https://doi.org/10.1021/jz500737m>.
- [24] Yudong Qiu, Paul S. Nerenberg, Teresa Head-Gordon, and Lee-Ping Wang. Systematic optimization of water models using liquid/vapor surface tension data. *The Journal of Physical Chemistry B*, 123(32):7061–7073, July 2019. doi: 10.1021/acs.jpcc.9b05455. URL <https://doi.org/10.1021/acs.jpcc.9b05455>.
- [25] Adam Paszke, Sam Gross, Francisco Massa, Adam Lerer, James Bradbury, Gregory Chanan, Trevor Killeen, Zeming Lin, Natalia Gimelshein, Luca Antiga, Alban Desmaison, Andreas Kopf, Edward Yang, Zachary DeVito, Martin Raison, Alykhan Tejani, Sasank Chilamkurthy, Benoit Steiner, Lu Fang, Junjie Bai, and Soumith Chintala. Pytorch: An imperative style, high-performance deep learning library. In H. Wallach, H. Larochelle, A. Beygelzimer, F. d'Alché-Buc, E. Fox, and R. Garnett, editors, *Advances in Neural Information Processing Systems 32*, pages 8024–8035. Curran Associates, Inc., 2019. URL <http://papers.neurips.cc/paper/9015-pytorch-an-imperative-style-high-performance-deep-learning-library.pdf>.
- [26] Martín Abadi, Ashish Agarwal, Paul Barham, Eugene Brevdo, Zhifeng Chen, Craig Citro, Greg S. Corrado, Andy Davis, Jeffrey Dean, Matthieu Devin, Sanjay Ghemawat, Ian Goodfellow, Andrew Harp, Geoffrey Irving, Michael Isard, Yangqing Jia, Rafal Jozefowicz, Lukasz Kaiser, Manjunath Kudlur, Josh Levenberg, Dandelion Mané, Rajat Monga, Sherry Moore, Derek Murray, Chris Olah, Mike Schuster, Jonathon Shlens, Benoit Steiner, Ilya Sutskever, Kunal Talwar, Paul Tucker, Vincent Vanhoucke, Vijay Vasudevan, Fernanda Viégas, Oriol Vinyals, Pete Warden, Martin Wattenberg, Martin Wicke, Yuan Yu, and Xiaoqiang Zheng. TensorFlow: Large-scale machine learning on heterogeneous systems, 2015. URL <https://www.tensorflow.org/>. Software available from tensorflow.org.
- [27] James Bradbury, Roy Frostig, Peter Hawkins, Matthew James Johnson, Chris Leary, Dougal Maclaurin, George Nectula, Adam Paszke, Jake VanderPlas, Skye Wanderman-Milne, and Qiao Zhang. JAX: composable transformations of Python+NumPy programs, 2018. URL <http://github.com/google/jax>.
- [28] Keyulu Xu, Weihua Hu, Jure Leskovec, and Stefanie Jegelka. How powerful are graph neural networks? *arXiv preprint arXiv:1810.00826*, 2018.
- [29] Yuanqing Wang, Josh Fass, Chaya D Stern, Kun Luo, and John Chodera. Graph nets for partial charge prediction. *arXiv preprint arXiv:1909.07903*, 2019.
- [30] Thomas N. Kipf and Max Welling. Semi-supervised classification with graph convolutional networks. *CoRR*, abs/1609.02907, 2016. URL <http://arxiv.org/abs/1609.02907>.
- [31] Peter W Battaglia, Jessica B Hamrick, Victor Bapst, Alvaro Sanchez-Gonzalez, Vinicius Zambaldi, Mateusz Malinowski, Andrea Tacchetti, David Raposo, Adam Santoro, Ryan Faulkner, et al. Relational inductive biases, deep learning, and graph networks. *arXiv preprint arXiv:1806.01261*, 2018.
- [32] Jian Du, Shanghang Zhang, Guanhang Wu, Jose M. F. Moura, and Soumya Kar. Topology Adaptive Graph Convolutional Networks. *arXiv:1710.10370 [cs, stat]*, February 2018.
- [33] Felix Wu, Tianyi Zhang, Amauri Holanda de Souza Jr, Christopher Fifty, Tao Yu, and Kilian Q Weinberger. Simplifying graph convolutional networks. *arXiv preprint arXiv:1902.07153*, 2019.

- [34] Minjie Wang, Da Zheng, Zihao Ye, Quan Gan, Mufei Li, Xiang Song, Jinjing Zhou, Chao Ma, Lingfan Yu, Yu Gai, et al. Deep graph library: A graph-centric, highly-performant package for graph neural networks. *arXiv preprint arXiv:1909.01315*, 2019.
- [35] Yue Wang, Yongbin Sun, Ziwei Liu, Sanjay E Sarma, Michael M Bronstein, and Justin M Solomon. Dynamic graph cnn for learning on point clouds. *Acm Transactions On Graphics (tog)*, 38(5):1–12, 2019.
- [36] David K Duvenaud, Dougal Maclaurin, Jorge Iparraguirre, Rafael Bombarell, Timothy Hirzel, Alán Aspuru-Guzik, and Ryan P Adams. Convolutional networks on graphs for learning molecular fingerprints. In *Advances in neural information processing systems*, pages 2224–2232, 2015.
- [37] Justin Gilmer, Samuel S Schoenholz, Patrick F Riley, Oriol Vinyals, and George E Dahl. Neural message passing for quantum chemistry. In *International conference on machine learning*, pages 1263–1272. PMLR, 2017.
- [38] Chaya D Stern, Christopher I Bayly, Daniel GA Smith, Josh Fass, Lee-Ping Wang, David L Mobley, and John D Chodera. Capturing non-local through-bond effects when fragmenting molecules for quantum chemical torsion scans. *bioRxiv*, 2020.
- [39] Tsz Wai Ko, Jonas A Finkler, Stefan Goedecker, and Jörg Behler. A fourth-generation high-dimensional neural network potential with accurate electrostatics including non-local charge transfer. *Nature communications*, 12(1):1–11, 2021.
- [40] Jon R Maple, M-J Hwang, Thomas P. Stockfisch, Uri Dinur, Marvin Waldman, Carl S Ewig, and Arnold T. Hagler. Derivation of class ii force fields. i. methodology and quantum force field for the alkyl functional group and alkane molecules. *Journal of Computational Chemistry*, 15(2):162–182, 1994.
- [41] Mj J Hwang, TP Stockfisch, and AT Hagler. Derivation of class ii force fields. 2. derivation and characterization of a class ii force field, cff93, for the alkyl functional group and alkane molecules. *Journal of the American Chemical Society*, 116(6):2515–2525, 1994.
- [42] JR Maple, M-J Hwang, TP Stockfisch, and AT Hagler. Derivation of class ii force fields. iii. characterization of a quantum force field for alkanes. *Israel Journal of Chemistry*, 34(2):195–231, 1994.
- [43] Zhengwei Peng, Carl S Ewig, Ming-Jing Hwang, Marvin Waldman, and Arnold T Hagler. Derivation of class ii force fields. 4. van der waals parameters of alkali metal cations and halide anions. *The Journal of Physical Chemistry A*, 101(39):7243–7252, 1997.
- [44] JR Maple, M-J Hwang, Karl James Jalkanen, Thomas P Stockfisch, and Arnold T Hagler. Derivation of class ii force fields: V. quantum force field for amides, peptides, and related compounds. *Journal of computational chemistry*, 19(4):430–458, 1998.
- [45] Pnina Dauber-Osguthorpe and Arnold T Hagler. Biomolecular force fields: where have we been, where are we now, where do we need to go and how do we get there? *Journal of computer-aided molecular design*, 33(2):133–203, 2019.
- [46] Arnold T Hagler. Force field development phase ii: Relaxation of physics-based criteria... or inclusion of more rigorous physics into the representation of molecular energetics. *Journal of computer-aided molecular design*, 33(2): 205–264, 2019.
- [47] James A Maier, Carmenza Martinez, Koushik Kasavajhala, Lauren Wickstrom, Kevin E Hauser, and Carlos Simmerling. ff14sb: improving the accuracy of protein side chain and backbone parameters from ff99sb. *Journal of chemical theory and computation*, 11(8):3696–3713, 2015.
- [48] Robert B Best, Xiao Zhu, Jihyun Shim, Pedro EM Lopes, Jeetain Mittal, Michael Feig, and Alexander D MacKerell Jr. Optimization of the additive charmm all-atom protein force field targeting improved sampling of the backbone  $\phi$ ,  $\psi$  and side-chain  $\chi_1$  and  $\chi_2$  dihedral angles. *Journal of chemical theory and computation*, 8(9):3257–3273, 2012.
- [49] Jérôme Delhommelle and Philippe Millié. Inadequacy of the lorentz-berthelot combining rules for accurate predictions of equilibrium properties by molecular simulation. *Molecular Physics*, 99(8):619–625, 2001.
- [50] Marvin Waldman and Arnold T Hagler. New combining rules for rare gas van der waals parameters. *Journal of computational chemistry*, 14(9):1077–1084, 1993.
- [51] Christopher M Baker, Pedro EM Lopes, Xiao Zhu, Benoît Roux, and Alexander D MacKerell Jr. Accurate calculation of hydration free energies using pair-specific lennard-jones parameters in the charmm drude polarizable force field. *Journal of chemical theory and computation*, 6(4):1181–1198, 2010.

- [52] Junmei Wang, Romain M Wolf, James W Caldwell, Peter A Kollman, and David A Case. Development and testing of a general amber force field. *Journal of computational chemistry*, 25(9):1157–1174, 2004.
- [53] Junmei Wang, Wei Wang, Peter A Kollman, and David A Case. Automatic atom type and bond type perception in molecular mechanical calculations. *Journal of molecular graphics and modelling*, 25(2):247–260, 2006.
- [54] Kenno Vanommeslaeghe and Alexander D MacKerell Jr. Automation of the charmm general force field (cgenff) i: bond perception and atom typing. *Journal of chemical information and modeling*, 52(12):3144–3154, 2012.
- [55] Kenno Vanommeslaeghe, E Prabhu Raman, and Alexander D MacKerell Jr. Automation of the charmm general force field (cgenff) ii: assignment of bonded parameters and partial atomic charges. *Journal of chemical information and modeling*, 52(12):3155–3168, 2012.
- [56] B Weisfeiler and A Leman. The reduction of a graph to canonical form and the algebra which appears therein. 1968.
- [57] Yudong Qiu, Daniel Smith, Simon Boothroyd, Hyesu Jang, Jeffrey Wagner, Caitlin C. Bannan, Trevor Gokey, Victoria T. Lim, Chaya Stern, Andrea Rizzi, and et al. Development and benchmarking of open force field v1.0.0, the parsley small molecule force field. *ChemRxiv*, 2021. doi: 10.33774/chemrxiv-2021-10701-v4.
- [58] Ryan L. Murphy, Balasubramaniam Srinivasan, Vinayak A. Rao, and Bruno Ribeiro. Janosy pooling: Learning deep permutation-invariant functions for variable-size inputs. *CoRR*, abs/1811.01900, 2018. URL <http://arxiv.org/abs/1811.01900>.
- [59] Hyesu Jang, Jessica Maat, Yudong Qiu, Daniel G.A. Smith, Simon Boothroyd, Jeffrey Wagner, Caitlin C. Bannan, Trevor Gokey, Victoria T. Lim, Xavier Lucas, and et al. openforcefield/openforcefields: Version 1.2.0 "parsley" update. Jun 2020. doi: 10.5281/zenodo.3872244.
- [60] Thomas A Halgren. The representation of van der waals (vdw) interactions in molecular mechanics force fields: potential form, combination rules, and vdw parameters. *Journal of the American Chemical Society*, 114(20):7827–7843, 1992.
- [61] Pengyu Ren and Jay W Ponder. Consistent treatment of inter-and intramolecular polarization in molecular mechanics calculations. *Journal of computational chemistry*, 23(16):1497–1506, 2002.
- [62] Justin A Lemkul, Jing Huang, Benoît Roux, and Alexander D MacKerell Jr. An empirical polarizable force field based on the classical drude oscillator model: development history and recent applications. *Chemical reviews*, 116(9):4983–5013, 2016.
- [63] Itai Leven and Teresa Head-Gordon. C-gem: Coarse-grained electron model for predicting the electrostatic potential in molecules. *The journal of physical chemistry letters*, 10(21):6820–6826, 2019.
- [64] Jon R Maple, M-J Hwang, Thomas P. Stockfisch, Uri Dinur, Marvin Waldman, Carl S Ewig, and Arnold T. Hagler. Derivation of class ii force fields. i. methodology and quantum force field for the alkyl functional group and alkane molecules. *Journal of Computational Chemistry*, 15(2):162–182, 1994.
- [65] Mj J Hwang, TP Stockfisch, and AT Hagler. Derivation of class ii force fields. 2. derivation and characterization of a class ii force field, cff93, for the alkyl functional group and alkane molecules. *Journal of the American Chemical Society*, 116(6):2515–2525, 1994.
- [66] JR Maple, M-J Hwang, TP Stockfisch, and AT Hagler. Derivation of class ii force fields. iii. characterization of a quantum force field for alkanes. *Israel Journal of Chemistry*, 34(2):195–231, 1994.
- [67] Kenno Vanommeslaeghe, Mingjun Yang, and Alexander D. MacKerell Jr. Robustness in the fitting of molecular mechanics parameters. *Journal of Computational Chemistry*, 36(14):1083–1101, 2015. doi: <https://doi.org/10.1002/jcc.23897>. URL <https://onlinelibrary.wiley.com/doi/abs/10.1002/jcc.23897>.
- [68] Lee-Ping Wang, Jiahao Chen, and Troy Van Voorhis. Systematic parametrization of polarizable force fields from quantum chemistry data. *Journal of chemical theory and computation*, 9(1):452–460, 2013.
- [69] Lee-Ping Wang, Todd J Martinez, and Vijay S Pande. Building force fields: An automatic, systematic, and reproducible approach. *The journal of physical chemistry letters*, 5(11):1885–1891, 2014.
- [70] Anders S. Christensen and O. Anatole von Lilienfeld. On the role of gradients for machine learning of molecular energies and forces, 2020.

- [71] Stefan Chmiela, Huziel E. Sauceda, Igor Poltavsky, Klaus-Robert Müller, and Alexandre Tkatchenko. sgdml: Constructing accurate and data efficient molecular force fields using machine learning. *Computer Physics Communications*, 240:38–45, 2019. doi: 10.1016/j.cpc.2019.02.007.
- [72] Huziel E. Sauceda, Stefan Chmiela, Igor Poltavsky, Klaus-Robert Müller, and Alexandre Tkatchenko. Molecular force fields with gradient-domain machine learning: Construction and application to dynamics of small molecules with coupled cluster forces. *The Journal of Chemical Physics*, 150(11):114102, 2019. doi: 10.1063/1.5078687.
- [73] Huziel E. Sauceda, Michael Gastegger, Stefan Chmiela, Klaus-Robert Müller, and Alexandre Tkatchenko. Molecular force fields with gradient-domain machine learning (gdml): Comparison and synergies with classical force fields, 2020.
- [74] Hans W Horn, William C Swope, Jed W Pitera, Jeffrey D Madura, Thomas J Dick, Greg L Hura, and Teresa Head-Gordon. Development of an improved four-site water model for biomolecular simulations: Tip4p-ew. *The Journal of chemical physics*, 120(20):9665–9678, 2004.
- [75] Lee-Ping Wang, Keri A McKiernan, Joseph Gomes, Kyle A Beauchamp, Teresa Head-Gordon, Julia E Rice, William C Swope, Todd J Martínez, and Vijay S Pande. Building a more predictive protein force field: a systematic and reproducible route to amber-fb15. *The Journal of Physical Chemistry B*, 121(16):4023–4039, 2017.
- [76] Eliot Boulanger, Lei Huang, Chetan Rupakheti, Alexander D MacKerell Jr, and Benoît Roux. Optimized lennard-jones parameters for druglike small molecules. *Journal of chemical theory and computation*, 14(6):3121–3131, 2018.
- [77] SimonBoothroyd, Owen Madin, Jeff Wagner, Jeffrey Setiadi, Jaime Rodríguez-Guerra, Matt Thompson, and David Dotson. openforcefield/openff-evaluator: 0.3.0, October 2020. URL <https://doi.org/10.5281/zenodo.4153484>.
- [78] Kristof Schütt, Pieter-Jan Kindermans, Huziel Enoc Sauceda Felix, Stefan Chmiela, Alexandre Tkatchenko, and Klaus-Robert Müller. Schnet: A continuous-filter convolutional neural network for modeling quantum interactions. In *Advances in neural information processing systems*, pages 991–1001, 2017.
- [79] Kun Yao, John E. Herr, David W. Toth, Ryker Mckintyre, and John Parkhill. The tensormol-0.1 model chemistry: a neural network augmented with long-range physics. *Chem. Sci.*, 9:2261–2269, 2018. doi: 10.1039/C7SC04934J. URL <http://dx.doi.org/10.1039/C7SC04934J>.
- [80] Kenno Vanommeslaeghe, E Prabhu Raman, and Alexander D MacKerell Jr. Automation of the charmm general force field (cgenff) ii: assignment of bonded parameters and partial atomic charges. *Journal of chemical information and modeling*, 52(12):3155–3168, 2012.
- [81] Kenno Vanommeslaeghe, E Prabhu Raman, and Alexander D MacKerell Jr. Automation of the charmm general force field (cgenff) ii: assignment of bonded parameters and partial atomic charges. *Journal of chemical information and modeling*, 52(12):3155–3168, 2012.
- [82] John J Irwin and Brian K Shoichet. Zinc- a free database of commercially available compounds for virtual screening. *Journal of chemical information and modeling*, 45(1):177–182, 2005.
- [83] An informal amber small molecule force field: parm@frosst, 2010. URL [http://www.ccl.net/cca/data/parm\\_at\\_Frosst/](http://www.ccl.net/cca/data/parm_at_Frosst/).
- [84] Junmei Wang, Romain M. Wolf, James W. Caldwell, Peter A. Kollman, and David A. Case. Development and testing of a general amber force field. *Journal of Computational Chemistry*, 25(9):1157–1174, 2004. doi: 10.1002/jcc.20035. URL <https://onlinelibrary.wiley.com/doi/abs/10.1002/jcc.20035>.
- [85] Caitlin C. Bannan and David Mobley. ChemPer: An Open Source Tool for Automatically Generating SMIRKS Patterns. 6 2019. doi: 10.26434/chemrxiv.8304578.v1. URL [https://chemrxiv.org/articles/preprint/ChemPer\\_An\\_Open\\_Source\\_Tool\\_for\\_Automatically\\_Generating\\_SMIRKS\\_Patterns/8304578](https://chemrxiv.org/articles/preprint/ChemPer_An_Open_Source_Tool_for_Automatically_Generating_SMIRKS_Patterns/8304578).
- [86] Trevor Gokey. Openff sandbox cho phalkethoh v1.0, 2020. URL <https://github.com/openforcefield/qca-dataset-submission/tree/master/submissions/2020-09-18-OpenFF-Sandbox-CHO-PhAlkEthOH>.
- [87] Jeff Wagner, David L. Mobley, Matt Thompson, John Chodera, Caitlin Bannan, Andrea Rizzi, trevogokey, David Dotson, Jaime Rodríguez-Guerra, Camila, Pavan Behara, Christopher Bayly, Josh A. Mitchell, Josh Horton, Nathan M. Lim, Victoria Lim, Sukanya Sasmal, Lily Wang, Andrew Dalke, SimonBoothroyd, Iván Pulido, Daniel Smith, Lee-Ping Wang, and Yutong Zhao. openforcefield/openff-toolkit: 0.10.0 Improvements for force field fitting, August 2021. URL <https://doi.org/10.5281/zenodo.5153946>.

- [88] David L Mobley, Caitlin C Bannan, Andrea Rizzi, Christopher I Bayly, John D Chodera, Victoria T Lim, Nathan M Lim, Kyle A Beauchamp, Michael R Shirts, Michael K Gilson, et al. Open force field consortium: Escaping atom types using direct chemical perception with smirnoff v0. 1. *BioRxiv*, page 286542, 2018.
- [89] Daniel GA Smith, Doaa Altarawy, Lori A Burns, Matthew Welborn, Levi N Naden, Logan Ward, Sam Ellis, Benjamin P Pritchard, and T Daniel Crawford. The molssi qcarchive project: An open-source platform to compute, organize, and share quantum chemistry data. *Wiley Interdisciplinary Reviews: Computational Molecular Science*, page e1491, 2020.
- [90] Yudong Qiu, Daniel Smith, Simon Boothroyd, Hyesu Jang, Jeffrey Wagner, Caitlin C Bannan, Trevor Gokey, Victoria T Lim, Chaya Stern, Andrea Rizzi, et al. Development and benchmarking of open force field v1. 0.0, the parsley small molecule force field. 2021.
- [91] William R. Pitt, David M. Parry, Benjamin G. Perry, and Colin R. Groom. Heteroaromatic rings of the future. *Journal of Medicinal Chemistry*, 52(9):2952–2963, 2009. doi: 10.1021/jm801513z. URL <https://doi.org/10.1021/jm801513z>. PMID: 19348472.
- [92] Viki Kumar Prasad, Alberto Otero-de-la Roza, and Gino A. DiLabio. Pepconf, a diverse data set of peptide conformational energies, Jan 2019. URL <https://doi.org/10.1038/sdata.2018.310>.
- [93] Jeff Wagner, Matt Thompson, David Dotson, hyejang, and Jaime Rodríguez-Guerra. openforcefield/openforcefields: Version 1.2.1 "Parsley" Update, September 2020. URL <https://doi.org/10.5281/zenodo.4021623>.
- [94] Wendy D Cornell, Piotr Cieplak, Christopher I Bayly, Ian R Gould, Kenneth M Merz, David M Ferguson, David C Spellmeyer, Thomas Fox, James W Caldwell, and Peter A Kollman. A second generation force field for the simulation of proteins, nucleic acids, and organic molecules. *Journal of the American Chemical Society*, 117(19):5179–5197, 1995.
- [95] Yong Duan, Chun Wu, Shibasish Chowdhury, Mathew C Lee, Guoming Xiong, Wei Zhang, Rong Yang, Piotr Cieplak, Ray Luo, Taisung Lee, et al. A point-charge force field for molecular mechanics simulations of proteins based on condensed-phase quantum mechanical calculations. *Journal of computational chemistry*, 24(16):1999–2012, 2003.
- [96] David S Cerutti, Julia E Rice, William C Swope, and David A Case. Derivation of fixed partial charges for amino acids accommodating a specific water model and implicit polarization. *The Journal of Physical Chemistry B*, 117(8):2328–2338, 2013.
- [97] Karl T Debiec, David S Cerutti, Lewis R Baker, Angela M Gronenborn, David A Case, and Lillian T Chong. Further along the road less traveled: Amber ff15ipq, an original protein force field built on a self-consistent physical model. *Journal of chemical theory and computation*, 12(8):3926–3947, 2016.
- [98] Araz Jakalian, Bruce L Bush, David B Jack, and Christopher I Bayly. Fast, efficient generation of high-quality atomic charges. am1-bcc model: I. method. *Journal of computational chemistry*, 21(2):132–146, 2000.
- [99] Araz Jakalian, David B Jack, and Christopher I Bayly. Fast, efficient generation of high-quality atomic charges. am1-bcc model: II. parameterization and validation. *Journal of computational chemistry*, 23(16):1623–1641, 2002.
- [100] Christopher I Bayly, Piotr Cieplak, Wendy Cornell, and Peter A Kollman. A well-behaved electrostatic potential based method using charge restraints for deriving atomic charges: the resp model. *The Journal of Physical Chemistry*, 97(40):10269–10280, 1993.
- [101] Michael Schauerl, Paul S Nerenberg, Hyesu Jang, Lee-Ping Wang, Christopher I Bayly, David L Mobley, and Michael K Gilson. Non-bonded force field model with advanced restrained electrostatic potential charges (resp2). *Communications Chemistry*, 3(1):1–11, 2020.
- [102] George A Khoury, Jeff P Thompson, James Smadbeck, Chris A Kieslich, and Christodoulos A Floudas. Forcefield\_ptm: Ab initio charge and amber forcefield parameters for frequently occurring post-translational modifications. *Journal of chemical theory and computation*, 9(12):5653–5674, 2013.
- [103] Patrick Bleiziffer, Kay Schaller, and Sereina Riniker. Machine learning of partial charges derived from high-quality quantum-mechanical calculations. *Journal of chemical information and modeling*, 58(3):579–590, 2018.
- [104] Nicholas Lubbers, Justin S Smith, and Kipton Barros. Hierarchical modeling of molecular energies using a deep neural network. *The Journal of chemical physics*, 148(24):241715, 2018.
- [105] Andrew E Sifain, Nicholas Lubbers, Benjamin T Nebgen, Justin S Smith, Andrey Y Lokhov, Olexandr Isayev, Adrian E Roitberg, Kipton Barros, and Sergei Tretiak. Discovering a transferable charge assignment model using machine learning. *The journal of physical chemistry letters*, 9(16):4495–4501, 2018.

- [106] Anthony K Rappe and William A Goddard III. Charge equilibration for molecular dynamics simulations. *The Journal of Physical Chemistry*, 95(8):3358–3363, 1991.
- [107] Michael K Gilson, Hillary SR Gilson, and Michael J Potter. Fast assignment of accurate partial atomic charges: an electronegativity equalization method that accounts for alternate resonance forms. *Journal of chemical information and computer sciences*, 43(6):1982–1997, 2003.
- [108] Peter Eastman and Vijay Pande. Accelerating development and execution speed with just-in-time gpu code generation. In *GPU Computing Gems Jade Edition*, pages 399–407. Elsevier, 2012.
- [109] D.A. Case, K. Belfon, I.Y. Ben-Shalom, S.R. Brozell, D.S. Cerutti, T.E. Cheatham, III, V.W.D. Cruzeiro, T.A. Darden, R.E. Duke, G. Giambasu, M.K. Gilson, H. Gohlke, R Harris A.W. Goetz, S. Izadi, S.A. Izmailov, K. Kasavajhala, A. Kovalevko, R. Krasny, T. Kurtzman, T.S. Lee, S. LeGrand, P. Li, C. Lin, J. Liu, T. Luchko, R. Luo, V. Man, K.M. Merz, Y. Miao, O. Mikhailovskii, G. Monard, H. Nguyen, A. Onufriev, F. Pan, S. Pantano, R. Qi, D.R. Roe, A. Roitberg, C. Sagui, S. Schott-Verdugo, J. Shen, C.L. Simmerling, N.R. Skrynnikov, J. Smith, J. Swails, R.C. Walker, J. Wang, L. Wilson, R.M. Wolf, X. Wu, Y. Xiong, Y. Xue, D.M. York, and P.A. Kollman. Amber 2020, 2020.
- [110] Yudong Qiu, Daniel Smith, Simon Boothroyd, Hyesu Jang, Jeffrey Wagner, Caitlin C Bannan, Trevor Gokey, Victoria T Lim, Chaya Stern, Andrea Rizzi, et al. Development and benchmarking of open force field v1. 0.0, the parsley small molecule force field. 2020.
- [111] Viki Kumar Prasad, Alberto Otero-de La-Roza, and Gino A DiLabio. Pepconf, a diverse data set of peptide conformational energies. *Scientific data*, 6:180310, 2019.
- [112] Antonia SJS Mey, Bryce Allen, Hannah E Bruce Macdonald, John D Chodera, Maximilian Kuhn, Julien Michel, David L Mobley, Levi N Naden, Samarjeet Prasad, Andrea Rizzi, et al. Best practices for alchemical free energy calculations. *arXiv preprint arXiv:2008.03067*, 2020.
- [113] William L Jorgensen, Jayaraman Chandrasekhar, Jeffrey D Madura, Roger W Impey, and Michael L Klein. Comparison of simple potential functions for simulating liquid water. *The Journal of chemical physics*, 79(2):926–935, 1983.
- [114] In Suk Joung and Thomas E Cheatham III. Determination of alkali and halide monovalent ion parameters for use in explicitly solvated biomolecular simulations. *The journal of physical chemistry B*, 112(30):9020–9041, 2008.
- [115] Rodrigo Galindo-Murillo, James C Robertson, Marie Zgarbova, Jiri Sponer, Michal Otyepka, Petr Jurecka, and Thomas E Cheatham III. Assessing the current state of amber force field modifications for dna. *Journal of chemical theory and computation*, 12(8):4114–4127, 2016.
- [116] Alberto Pérez, Iván Marchán, Daniel Svozil, Jiri Sponer, Thomas E Cheatham III, Charles A Loughton, and Modesto Orozco. Refinement of the amber force field for nucleic acids: improving the description of  $\alpha/\gamma$  conformers. *Bio-physical journal*, 92(11):3817–3829, 2007.
- [117] In Suk Joung and Thomas E Cheatham III. Molecular dynamics simulations of the dynamic and energetic properties of alkali and halide ions using water-model-specific ion parameters. *The Journal of Physical Chemistry B*, 113(40):13279–13290, 2009.
- [118] Pengfei Li, Benjamin P Roberts, Dhruva K Chakravorty, and Kenneth M Merz Jr. Rational design of particle mesh ewald compatible lennard-jones parameters for + 2 metal cations in explicit solvent. *Journal of chemical theory and computation*, 9(6):2733–2748, 2013.
- [119] Pengfei Li and Kenneth M Merz Jr. Taking into account the ion-induced dipole interaction in the nonbonded model of ions. *Journal of chemical theory and computation*, 10(1):289–297, 2014.
- [120] Pengfei Li, Lin Frank Song, and Kenneth M Merz Jr. Parameterization of highly charged metal ions using the 12-6-4 lj-type nonbonded model in explicit water. *The Journal of Physical Chemistry B*, 119(3):883–895, 2015.
- [121] Callum J Dickson, Benjamin D Madej, Åge A Skjevik, Robin M Betz, Knut Teigen, Ian R Gould, and Ross C Walker. Lipid14: the amber lipid force field. *Journal of chemical theory and computation*, 10(2):865–879, 2014.
- [122] Karl N Kirschner, Austin B Yongye, Sarah M Tschampel, Jorge González-Outeiriño, Charlisha R Daniels, B Lachele Foley, and Robert J Woods. Glycam06: a generalizable biomolecular force field. carbohydrates. *Journal of computational chemistry*, 29(4):622–655, 2008.
- [123] Mari L DeMarco and Robert J Woods. Atomic-resolution conformational analysis of the gm3 ganglioside in a lipid bilayer and its implications for ganglioside–protein recognition at membrane surfaces. *Glycobiology*, 19(4):344–355, 2009.

- [124] Mari L DeMarco, Robert J Woods, James H Prestegard, and Fang Tian. Presentation of membrane-anchored glycosphingolipids determined from molecular dynamics simulations and nmr paramagnetic relaxation rate enhancement. *Journal of the American Chemical Society*, 132(4):1334–1338, 2010.
- [125] Dazhi Tan, Stefano Piana, Robert M Dirks, and David E Shaw. Rna force field with accuracy comparable to state-of-the-art protein force fields. *Proceedings of the National Academy of Sciences*, 115(7):E1346–E1355, 2018.
- [126] Shama Khan, Imane Bjjj, Fisayo A Olotu, Clement Agoni, Emmanuel Adeniji, and Mahmoud E S Soliman. Covalent simulations of covalent/irreversible enzyme inhibition in drug discovery: a reliable technical protocol. *Future medicinal chemistry*, 10(19):2265–2275, 2018.
- [127] Joseph D Yesselman, Daniel J Price, Jennifer L Knight, and Charles L Brooks III. Match: An atom-typing toolset for molecular mechanics force fields. *Journal of computational chemistry*, 33(2):189–202, 2012.
- [128] William L Jorgensen, David S Maxwell, and Julian Tirado-Rives. Development and testing of the opls all-atom force field on conformational energetics and properties of organic liquids. *Journal of the American Chemical Society*, 118(45):11225–11236, 1996.
- [129] Jian Yin, Andrew T Fenley, Niel M Henriksen, and Michael K Gilson. Toward improved force-field accuracy through sensitivity analysis of host-guest binding thermodynamics. *The Journal of Physical Chemistry B*, 119(32):10145–10155, 2015.
- [130] Niel M Henriksen and Michael K Gilson. Evaluating force field performance in thermodynamic calculations of cyclodextrin host-guest binding: Water models, partial charges, and host force field parameters. *Journal of chemical theory and computation*, 13(9):4253–4269, 2017.
- [131] Caitlin C Bannan, Kalistyn H Burley, Michael Chiu, Michael R Shirts, Michael K Gilson, and David L Mobley. Blind prediction of cyclohexane-water distribution coefficients from the sampl5 challenge. *Journal of computer-aided molecular design*, 30(11):927–944, 2016.
- [132] Mehtap Işık, Teresa Danielle Bergazin, Thomas Fox, Andrea Rizzi, John D Chodera, and David L Mobley. Assessing the accuracy of octanol-water partition coefficient predictions in the sampl6 part ii log p challenge. *Journal of Computer-Aided Molecular Design*, pages 1–36, 2020.
- [133] Andrew S Paluch, Sreeja Parameswaran, Shuai Liu, Anasuya Kolavennu, and David L Mobley. Predicting the excess solubility of acetanilide, acetaminophen, phenacetin, benzocaine, and caffeine in binary water/ethanol mixtures via molecular simulation. *The Journal of chemical physics*, 142(4):01B621\_1, 2015.
- [134] Shuai Liu, Shannon Cao, Kevin Hoang, Kayla L Young, Andrew S Paluch, and David L Mobley. Using md simulations to calculate how solvents modulate solubility. *Journal of chemical theory and computation*, 12(4):1930–1941, 2016.
- [135] Guilherme Duarte Ramos Matos, Gaetano Calabro, and David L Mobley. Infinite dilution activity coefficients as constraints for force field parametrization and method development. *Journal of chemical theory and computation*, 15(5):3066–3074, 2019.
- [136] Michael R Shirts and John D Chodera. Statistically optimal analysis of samples from multiple equilibrium states. *The Journal of chemical physics*, 129(12):124105, 2008.
- [137] Marcus Wieder, Josh Fass, and John D Chodera. Teaching free energy calculations to learn from experimental data. *bioRxiv*, 2021.
- [138] J Peter Toennies. On the validity of a modified buckingham potential for the rare gas dimers at intermediate distances. *Chemical Physics Letters*, 20(3):238–241, 1973.
- [139] Tom Darden, Darrin York, and Lee Pedersen. Particle mesh ewald: An nlog (n) method for ewald sums in large systems. *The Journal of chemical physics*, 98(12):10089–10092, 1993.
- [140] Alžbeta Kubincová, Sereina Riniker, and Philippe H Hünenberger. Reaction-field electrostatics in molecular dynamics simulations: Development of a conservative scheme compatible with an atomic cutoff. *Physical Chemistry Chemical Physics*, 22(45):26419–26437, 2020.
- [141] O Anatole Von Lilienfeld. Quantum machine learning in chemical compound space. *Angewandte Chemie International Edition*, 57(16):4164–4169, 2018.
- [142] Oliver T Unke and Markus Meuwly. Physnet: A neural network for predicting energies, forces, dipole moments, and partial charges. *Journal of chemical theory and computation*, 15(6):3678–3693, 2019.

- [143] Alan Grossfield and Daniel M Zuckerman. Quantifying uncertainty and sampling quality in biomolecular simulations. *Annual reports in computational chemistry*, 5:23–48, 2009.
- [144] John D Chodera. A simple method for automated equilibration detection in molecular simulations. *Journal of chemical theory and computation*, 12(4):1799–1805, 2016.
- [145] Alan Grossfield, Paul N Patrone, Daniel R Roe, Andrew J Schultz, Daniel W Siderius, and Daniel M Zuckerman. Best practices for quantification of uncertainty and sampling quality in molecular simulations [article v1. 0]. *Living journal of computational molecular science*, 1(1), 2018.
- [146] Fabien Cailliez and Pascal Pernot. Statistical approaches to forcefield calibration and prediction uncertainty in molecular simulation. *The Journal of Chemical Physics*, 134(5):054124, February 2011. ISSN 0021-9606. doi: 10.1063/1.3545069.
- [147] Fabien Cailliez, Arnaud Bourasseau, and Pascal Pernot. Calibration of forcefields for molecular simulation: Sequential design of computer experiments for building cost-efficient kriging metamodels. *Journal of Computational Chemistry*, 35(2):130–149, January 2014. ISSN 1096-987X. doi: 10.1002/jcc.23475.
- [148] Panagiotis Angelikopoulos, Costas Papadimitriou, and Petros Koumoutsakos. Bayesian uncertainty quantification and propagation in molecular dynamics simulations: A high performance computing framework. *The Journal of Chemical Physics*, 137(14):144103, October 2012. ISSN 0021-9606. doi: 10.1063/1.4757266.
- [149] P. E. Hadjidoukas, P. Angelikopoulos, C. Papadimitriou, and P. Koumoutsakos. II4U: A high performance computing framework for Bayesian uncertainty quantification of complex models. *Journal of Computational Physics*, 284:1–21, March 2015. ISSN 0021-9991. doi: 10.1016/j.jcp.2014.12.006.
- [150] Ben Cooke and Scott C. Schmidler. Statistical Prediction and Molecular Dynamics Simulation. *Biophysical Journal*, 95(10):4497–4511, November 2008. ISSN 0006-3495. doi: 10.1529/biophysj.108.131623.
- [151] Xiaowang Zhou and Stephen M. Foiles. Uncertainty Quantification and Reduction of Molecular Dynamics Models. 2017. doi: 10.5772/intechopen.68507.
- [152] F. Rizzi, H. Najm, B. Debusschere, K. Sargsyan, M. Salloum, H. Adalsteinsson, and O. Knio. Uncertainty Quantification in MD Simulations. Part II: Bayesian Inference of Force-Field Parameters. *Multiscale Modeling & Simulation*, 10(4):1460–1492, January 2012. ISSN 1540-3459. doi: 10.1137/110853170.
- [153] S. Wu, P. Angelikopoulos, C. Papadimitriou, R. Moser, and P. Koumoutsakos. A hierarchical Bayesian framework for force field selection in molecular dynamics simulations. *Phil. Trans. R. Soc. A*, 374(2060):20150032, February 2016. ISSN 1364-503X, 1471-2962. doi: 10.1098/rsta.2015.0032.
- [154] Lina Kulakova, Georgios Arampatzis, Panagiotis Angelikopoulos, Panagiotis Chatzidoukas, Costas Papadimitriou, and Petros Koumoutsakos. Experimental data over quantum mechanics simulations for inferring the repulsive exponent of the Lennard-Jones potential in Molecular Dynamics. *arXiv:1705.08533 [physics, stat]*, May 2017.
- [155] Paul N. Patrone and Andrew Dienstfrey. Uncertainty Quantification for Molecular Dynamics. *arXiv:1801.02483 [physics]*, January 2018.
- [156] Stephen Wu, Panagiotis Angelikopoulos, Gerardo Tauriello, Costas Papadimitriou, and Petros Koumoutsakos. Fusing heterogeneous data for the calibration of molecular dynamics force fields using hierarchical Bayesian models. *The Journal of Chemical Physics*, 145(24):244112, December 2016. ISSN 0021-9606. doi: 10.1063/1.4967956.
- [157] Richard A. Messerly, Thomas A. Knotts, and W. Vincent Wilding. Uncertainty quantification and propagation of errors of the Lennard-Jones 12-6 parameters for n-alkanes. *The Journal of Chemical Physics*, 146(19):194110, May 2017. ISSN 0021-9606. doi: 10.1063/1.4983406.
- [158] Owen C. Madin, Simon Boothroyd, Richard A. Messerly, John D. Chodera, Josh Fass, and Michael R. Shirts. Bayesian inference-driven model parameterization and model selection for 2CLJQ fluid models. *arXiv:2105.07863 [physics, stat]*, September 2021.
- [159] Camila Zanette, Caitlin C. Bannan, Christopher I. Bayly, Josh Fass, Michael K. Gilson, Michael R. Shirts, John D. Chodera, and David L. Mobley. Toward Learned Chemical Perception of Force Field Typing Rules. *Journal of Chemical Theory and Computation*, 15(1):402–423, January 2019. ISSN 1549-9618. doi: 10.1021/acs.jctc.8b00821.
- [160] Radford M. Neal. *Bayesian Learning for Neural Networks*. Lecture Notes in Statistics. Springer-Verlag, New York, 1996. ISBN 978-0-387-94724-2. doi: 10.1007/978-1-4612-0745-0.

- [161] Adam Paszke, Sam Gross, Soumith Chintala, Gregory Chanan, Edward Yang, Zachary DeVito, Zeming Lin, Alban Desmaison, Luca Antiga, and Adam Lerer. Automatic differentiation in pytorch. 2017.
- [162] Jeff Wagner, David L. Mobley, Caitlin Bannan, John Chodera, Andrea Rizzi, Matt Thompson, Josh Horton, David Dotson, Jaime Rodríguez-Guerra, Camila, Christopher Bayly, Josh Horton, trevorgokey, Nathan M. Lim, Victoria Lim, Pavan Behara, Simon Boothroyd, Sukanya Sasmal, Daniel Smith, Lee-Ping, and Yutong Zhao. openforcefield/openforcefield: 0.7.2 Bugfix and minor feature release, September 2020. URL <https://doi.org/10.5281/zenodo.4057038>.
- [163] Diederik P Kingma and Jimmy Ba. Adam: A method for stochastic optimization. *arXiv preprint arXiv:1412.6980*, 2014.
- [164] Will Hamilton, Zhitao Ying, and Jure Leskovec. Inductive representation learning on large graphs. In *Advances in neural information processing systems*, pages 1024–1034, 2017.
- [165] Felix Wu, Tianyi Zhang, Amauri H. Souza Jr., Christopher Fifty, Tao Yu, and Kilian Q. Weinberger. Simplifying graph convolutional networks. *CoRR*, abs/1902.07153, 2019. URL <http://arxiv.org/abs/1902.07153>.
- [166] Kurt Hornik. Approximation capabilities of multilayer feedforward networks. *Neural networks*, 4(2):251–257, 1991.
- [167] Kurt Hornik, Maxwell Stinchcombe, Halbert White, et al. Multilayer feedforward networks are universal approximators. 1991.

## 12 Acknowledgments

The authors wish to thank Yutong Zhao (0000-0003-0090-7801) for helpful feedback while troubleshooting implementations of molecular mechanics models automatic differentiation packages, and for helpful comments on the framing of this work. The authors wish to thank Christian L. Mueller (0000-0002-3821-7083).

## 13 Funding

YW acknowledges support from NSF CHI-1904822 and the Sloan Kettering Institute. JF acknowledges support from NSF CHE-1738979 and the Sloan Kettering Institute. JDC acknowledges support from NIH grant P30 CA008748, NIH grant R01 GM121505, NIH grant R01 GM132386, NSF CHI-1904822, and the Sloan Kettering Institute.

## 14 Disclosures

YW is among the co-founders and equity holders of Uli, Inc. and Uli (Shenzhen) Technology Co. Ltd.

JDC is a current member of the Scientific Advisory Board of OpenEye Scientific Software, Redesign Science, and Interline Therapeutics, and has equity interests in Redesign Science and Interline Therapeutics. The Chodera laboratory receives or has received funding from multiple sources, including the National Institutes of Health, the National Science Foundation, the Parker Institute for Cancer Immunotherapy, Relay Therapeutics, Entasis Therapeutics, Silicon Therapeutics, EMD Serono (Merck KGaA), AstraZeneca, Vir Biotechnology, Bayer, XtalPi, Interline Therapeutics, the Molecular Sciences Software Institute, the Starr Cancer Consortium, the Open Force Field Consortium, Cycle for Survival, a Louis V. Gerstner Young Investigator Award, and the Sloan Kettering Institute. A complete funding history for the Chodera lab can be found at <http://choderalab.org/funding>.

## 15 Disclaimers

The content is solely the responsibility of the authors and does not necessarily represent the official views of the National Institutes of Health.

## 16 Author Contributions

Conceptualization: JF, YW, JDC; Data Curation: YW, JF; Formal Analysis: YW; Funding Acquisition: JDC; Investigation: YW, JF; Methodology: YW, JF; Project Administration: JDC; Resources: JDC; Software: YW, JF; Supervision: JDC; Visualization: YW; Writing – Original Draft: YW; Writing – Review & Editing: YW, JDC, JF.

## 17 Appendix

### 18 Graph neural network (GNN) architectures considered in this paper

We considered the following graph neural network architectures available in DGL [34] in this paper:

Model	Edge update $\phi^e$	Edge aggregate $\rho^{e \rightarrow v}$	Node update $\phi^v$
GCN	Identity	Mean	NN
EdgeConv	$\text{ReLU}(W_0(\mathbf{v}_i - \mathbf{v}_j) + W_1\mathbf{v}_i)$	Max	Identity
GraphSAGE	Identity	Mean*	Normalize( $\text{NN}([\mathbf{v} : \mathbf{e}])$ )
GIN	Identity	Sum*	$\text{NN}((1 + \epsilon)\mathbf{v} + \mathbf{e})$

**Table 4. Summary of representative graph neural network architectures by edge update, edge aggregate, and node update types.** Models analyzed here include: GCN [30], EdgeConv [35], GraphSAGE [164], and GIN [28]. Other architectures evaluated—TAGCN [32] and SGC [33]—involve multi-step propagation, which could be expressed as a combination of these updates and aggregates.

\*: Multiple aggregation functions studied in the referenced publication.

## 19 Training losses

As mentioned in section 2.4, we can train the model using an arbitrary differentiable loss. Here, we describe the loss functions used in the reported experiments.

### 19.1 Classification loss

In Section 3, we used the cross-entropy loss, as implemented in PyTorch<sup>9</sup>, to reproduce GAFF 1.81 atom types.

## 20 Proof that Janossy pooling is sufficiently expressive

Now we prove that such formulation is expressive enough to distinguish bonds consisting of distinct atoms. An equivalent proof for angles and torsions follows similarly.

**Lemma 1.** *There exists a neural function  $\text{NN}_r$  such that,*

$$\text{NN}_r([h_{v_i} : h_{v_j}]) + \text{NN}_r([h_{v_j} : h_{v_i}]) = \text{NN}_r([h_{v_k} : h_{v_l}]) + \text{NN}_r([h_{v_l} : h_{v_k}])$$

*if and only if  $h_{v_i} = h_{v_l}$  and  $h_{v_j} = h_{v_k}$  or  $h_{v_i} = h_{v_k}$  and  $h_{v_j} = h_{v_l}$ .*

*Proof.* We first prove that there is a function  $f_r$  satisfying the condition in Lemma 1. With finite possible initial conditions and finite rounds of message passing, the possible values of  $h_v$  is finite (corresponding to the finite number of unique labels in Weisfeiler-Leman [56] test). We use  $c$  to denote the maximum value of the hash of  $h_v$ :

$$c = \max\{\text{hash}(h_v)\} \quad (36)$$

Thus, one example of such  $f_r : \mathbb{R}^D \rightarrow \mathbb{N}$  satisfying the condition in Lemma 1 is:

$$f_r(h_{v_i}, h_{v_j}) = \begin{cases} 0, & \text{hash}(h_{v_i}) \geq \text{hash}(h_{v_j}); \\ (c + 1)\text{hash}(h_{v_i}) + \text{hash}(h_{v_i}), & \text{hash}(h_{v_i}) < \text{hash}(h_{v_j}). \end{cases} \quad (37)$$

Following the universal approximation theorem [166, 167], there exists a neural function  $\text{NN}_r$  that approximates  $f_r$  arbitrarily well and thus satisfies the condition in Lemma 1.  $\square$

<sup>9</sup><https://pytorch.org/docs/stable/generated/torch.nn.CrossEntropyLoss.html#torch.nn.CrossEntropyLoss>

